

FINAL PUBLISHABLE REPORT

Grant Agreement number	14IND13
Project short name	PhotInd
Project full title	Metrology for the photonics industry - optical fibres, waveguides and applications
Period covered (dates)	From 1 August 2015 To 31 July 2018
Coordinator	
Name, title, organisation	Antti Lassila, Dr, VTT
Tel:	+358 40 7678584
Email:	antti.lassila@vtt.fi
Website address	https://www.photind.eu/
Other partners	
Short name, country	VTT, Finland Aalto, Finland CMI, Czech Republic CSIC, Spain Metrosert, Estonia NPL, United Kingdom Arden, United Kingdom FhG, Germany JCM, Germany Oplatek, Finland UEF, Finland UT, Estonia WWU, Germany Menlo, Germany METAS, Switzerland nLIGHT, Finland Seagate, United Kingdom Toptica, Germany

TABLE OF CONTENTS

1	Executive summary (not exceeding 1 page)	3
2	Need for the project.....	3
3	Objectives	3
4	Results	4
4.1	Develop traceable online and offline measurement techniques for dimensional and optical characterisation of advanced optical fibres and photonic components.....	4
4.2	Metrology for improved traceability of fibre-optic measuring instruments.....	12
4.3	Metrology of terahertz transmission links.....	25
4.4	Establish metrology tools for performance characterisation of polymer waveguides mounted on electronic circuit backplanes used in high-speed data links.....	29
5	Impact	42
5.1	Dissemination	42
5.2	Impact on industrial and other user communities	42
5.3	Impact on the metrology and scientific communities	43
5.4	Impact on relevant standards.....	44
5.5	Longer-term economic, social and environmental impacts.....	44
6	List of publications.....	46
7	Website address and contact details	48

1 Executive summary (not exceeding 1 page)

Optical fibres and other photonic components are being increasingly implemented in many rapidly-growing and demanding areas, such as aviation electronics, telecommunications and the automotive industry. New reliable measurement techniques and improved metrology are needed to meet these demands. The project developed online and offline measurement techniques for dimensional and optical characterisation of advanced photonic components and devices as well as the necessary calibration techniques and artefacts to enable calibration of the newest generation of measuring instruments. The developed characterisation and calibration techniques will underpin the development and manufacture of novel photonics components thereby strengthening the competitiveness of the European photonics industry, enabling innovation and providing faster, cheaper data connection.

2 Need for the project

The huge potential of photonics and fibre optics is evident from the Photonics21 Strategic Roadmap which lists the major photonic research and innovation challenges. One challenge has been that modern photonic systems utilise novel components, whose dimensional and optical properties cannot be reliably measured using current techniques: commercial instruments are often uncalibrated, provide insufficient accuracy and are available only for some of the required characteristics. Thus, new traceable and improved measurements and calibration methods were needed to make photonic measurement technology an enabling technology that will allow technological breakthroughs as well as commercialisation of sophisticated fibre optic components.

- Improving online measurements of dimensional parameters (diameters and concentricity) during fabrication will benefit manufacturing of special fibres and capillaries.
- Evaluation of the performance of photonic components in optical interconnects and the next-generation of microwave or THz transmission links, traceable measurements of key parameters (dynamic range, insertion loss, bandwidth, etc.) as well as industry standards is necessary.
- Development of traceable measurement techniques to study environmental effects on optical printed circuit boards the boards such as temperature cycling, ageing, humidity variation, etc. will help the data communications industry to understand the performance of optical printed circuit boards within their working environments.
- Coupling light without losses from fibres into optical circuits presents a challenge due to the large mode mismatch. Efficient solutions for matching conventional fibre-coupled systems to waveguides and nanophotonic devices are needed.
- Metrology for measuring modal distribution in multimode step-index optical fibres, as used in automotive systems, in industrial sensors and in medical applications is still not sufficient, leading to inconsistent measurement results that have a negative impact on the deployment of these systems.
- Novel optical fibre measuring instruments, like the high-resolution optical time-domain reflectometers, offer performances which cannot be adequately evaluated because of the lack of suitable calibration artefacts and procedures.

Optical communications, biophotonics, avionics, and automotive industries are examples of fields that will benefit from the improved measuring capabilities.

3 Objectives

The overall objective of the project is to develop new measurement techniques, improved metrology and standards to address the requirements of the manufacturers of state-of-the-art optical components and measurement devices.

The project addresses the following scientific and technical objectives:

1. **To develop traceable online and offline metrology techniques for dimensional and optical characterisation of advanced optical fibres and photonic components** – by developing measurement setups, procedures and the required numerical tools. Some of the most relevant dimensional parameters include the thicknesses of different layers of the fibre and the concentricity of different layers. The target accuracies for thickness and concentricity are 0.5 μm and 1 μm , respectively. Both simple and complex geometries will be investigated to determine the capabilities

of the developed measurement method. The work on optical parameters will focus on modern methods for dispersion measurements and the investigation of optical parameter measurements in high power applications. The goal is to measure the relative content of light in the core with an accuracy of $\pm 5\%$.

2. **To develop metrology for improved traceability of fibre optic measuring instruments** – by developing calibration techniques and artefacts. More specifically, the metrology of multimode fibres will be addressed, with the main goal to develop a measuring system for the Encircled Angular Flux (EAF) and to establish full traceability for this quantity, which is one of the key parameters allowing characterisation of modal distribution in multimode fibres and components. A further objective is to develop a series of artefacts for the calibration of the attenuation scale of multimode Optical Time Domain Reflectometers (OTDR) and also for the calibration of the distance scale with cm and/or mm resolution of high resolution single-mode and multimode OTDR, which belong to the most widespread optical fibre measuring instruments. This activity will also have a strong impact on the improvement of relevant calibration standards, such as those developed within the IEC. In addition, recent developments have shown the possibility to develop a novel portable absolute standard detector based on carbon nanotubes at cryogenic temperatures. These systems can solve the issues inherent to existing transfer standard detectors, like spectral dependence and temporal drift, and will shorten the traceability chain of optical power measurements. This will result in a lower measurement uncertainty (target accuracy better than 0.5%), thus addressing the emerging future needs of the fibre optics industry.
3. **To develop metrology of terahertz transmission links** – by developing measurement standards and standard measurement procedures for the traceable measurement of the key parameters of THz transmission links including the measurement of dynamic range, insertion loss, signal to noise ratio, bit error ratio (BER) for various modulation formats, free spectral range and bandwidth. The target accuracy for dynamic range and insertion loss measurements is 5% .
4. **To establish the metrology tools for performance characterisation of polymer waveguides mounted on electronic circuit backplanes used in high-speed data links** – by developing suitable measurement systems that can characterise the functional performance of waveguides incorporated onto short range interconnect boards. The systems will assess the key parameters of attenuation, isolation and BER, with respect to the functional and structural integrity of the entire interconnect board and the quality of the individual waveguides. The usability of typical fibre-to-fibre connectors at high average powers will be investigated. Towards this aim, the transmission as well as the heating of the components will be monitored (target accuracy: $\pm 5\%$). Measurement strategies to effectively characterise evaluation boards will be developed with accuracy levels within ~ 1 dB for attenuation.
5. **To engage with the European photonics industry and photonics equipment manufacturers** – to facilitate the take up of the technology and measurement techniques developed by the project, and to recommend what further actions are required to ensure uptake.

4 Results

4.1 Develop traceable online and offline measurement techniques for dimensional and optical characterisation of advanced optical fibres and photonic components

This objective included three aspects of fibre characterisation: development of measurement for online dimensional characterisation of optical fibres, development of modern methods for dispersion measurement, and high power fibre characterization.

4.1.1 Dimensional characterisation of advanced optical fibres

Currently available instruments can measure concentricity and diameter of optical fibre layers offline, typically by multi-directional laser scanning of the fibre immersed in index-matching oil, or by analysis of a polished fibre end, either directly with a microscope, or by using dark-field illumination. These methods are not suitable for monitoring or controlling the manufacturing process in real-time. In particular, there is a need for real-time evaluation of the geometry of a coating layer.

The project used the measurement principle based on analysis of forward scattering of a laser beam that illuminates the fibre transversely. This method was improved with modern detection and data analysis to allow measurements of more complex fibres and to reach higher resolution. The technique is based on continuously monitoring the resulting interference profile in a plane behind the fibre with a high-resolution linear detector, and determining the changes in fibre geometry based on the changes in the intensity distribution.

Generally, the position of the interference peaks in a fibre with refractive index of cladding (n_{clad}) higher than the refractive index or coating (n_{coat}) are correlated with a ratio of cladding to coating diameter $d_{\text{clad}}/d_{\text{coat}}$. As the ratio increases, the interference peaks move to larger angles, making the whole intensity profile wider. Deviations from concentricity of cladding to coating creates asymmetrical intensity profile. Since diameter and concentricity changes along the measurement axis have much smaller effect on the detected intensity distribution, two orthogonal channels are needed to monitor all changes in the fibre.

A 3D model of the measurement setup as well as a constructed prototype are shown in figure 1.1. VTT designed and constructed the prototype to meet the measurement requirements and target uncertainties defined by the optical fibre manufacturers Oplatek and nLIGHT. It consists of two horizontal detection channels, positioned orthogonally to each other. Oplatek and nLIGHT provided test samples for preliminary offline measurements. Online measurements were performed at Oplatek's premises, where an operational fibre drawing tower was available. The measured fibre runs vertically through the middle of the instrument, passing through both measurement beams. As the laser beam is hitting the fibre, it produces a dense interference pattern in all directions around the fibre, and thus the detection channels are positioned at different heights to avoid cross talk. The light source is a 633 nm HeNe laser, coupled into a fibre splitter, and collimated with two microscope objectives.

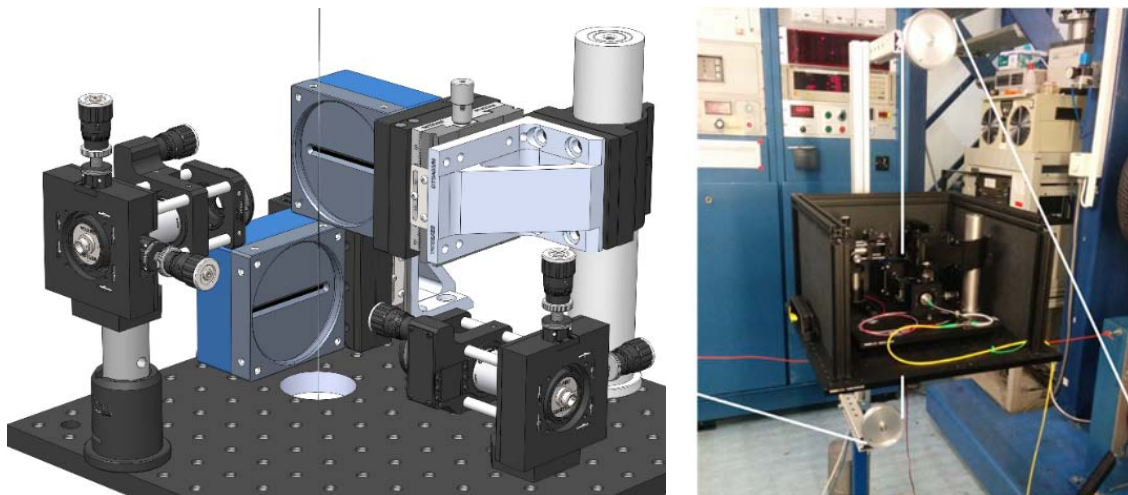


Figure 1.1. A model of the measurement setup at Oplatek's drawing tower, and a prototype instrument in production environment.

To measure the diffraction pattern two 12-bit monochrome linear array detectors are used, positioned such that in the absence of the fibre the measurement beam of each channel is incident on the centre of the respective sensor. Each detector is capturing approximately 90° angular range directly behind the fibre. The angular resolution in this configuration is between 0.015° (at the centres) to 0.008° (near the edges). Detectors were modified for the task by removing the protective glass in front of the sensors, because the thin glass was causing additional interference due to the coherence of the light source. The detectors were characterized for uniformity with a known illuminance source. The measured raw data is first corrected with uniformity calibration, then a smoothing filtering is applied, and finally the positions of the centre of the fibre and of the two outermost intensity peaks are recorded, as illustrated in figure 1.2.

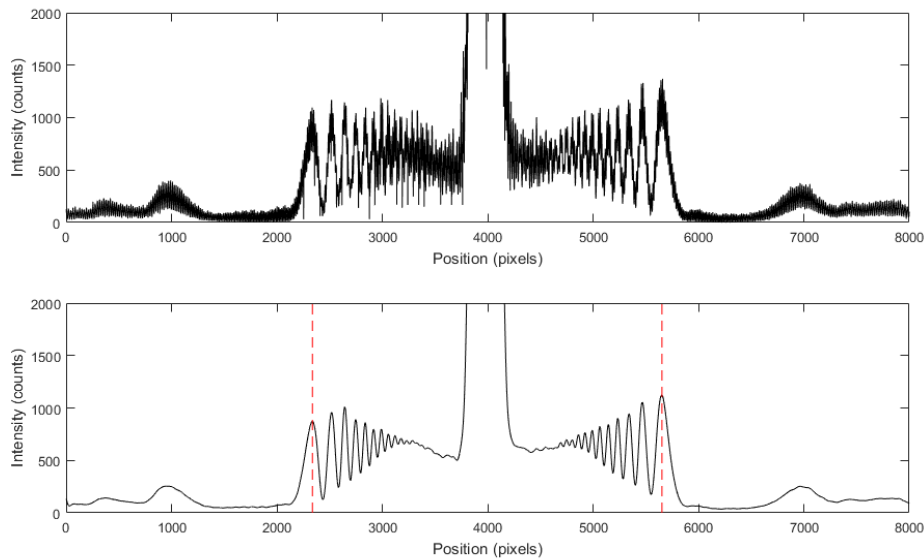


Figure 1.2. Example of the measured scattering profile (above), filtered data (below), and detected peak positions (red dashed lines).

Numerical methods for simulating advanced optical fibres were developed through discussions with UEF, JCM and CSIC, after the measurement configuration for dimensional characterisation of optical fibres was designed. Modelling of the laser beam propagation has been performed with Fourier Modal (FMM) by UEF, and finite-element methods (FEM) by JCM. Positions of the oscillation peaks correlate with the geometrical dimensions in the fibre. e.g., an increase in the ratio of glass diameter to the coating diameter widens the intensity profile, and decrease makes it narrower. Similarly, deviations from concentricity of layers affect the symmetry of the intensity profile. Both methods are computationally intensive, especially due to comparatively large size of the fibre compared to the wavelength of light. For example, a single FEM simulation takes approximately 30-40 minutes with a server grade computer, and FMM simulation takes upward of several hours.

Due to the time it takes to perform the simulation, neither method is currently suitable for online-applications. The calculations in this implementation are done in advance, by modelling the scattering profile for a nominal fibre geometry and for every deviation of interest. These models were done with FEM. From these results, the sensitivity parameters are calculated, which are used to determine the magnitude of deviations during the online measurements.

Test measurements were performed in the drawing tower for a single fibre type. The instrument was positioned between the tower and the spooling device, as illustrated in figure 1. The fibre type had a nominal glass diameter of 125 μm and two polymer coating layers of 195 μm and 260 μm diameters. The glass diameter was monitored before the coating process with a dedicated instrument. The calculated sensitivities of geometry changes to the selected interference peak position on the sensor were 60 nm/pixel for the coating diameter, and 15 nm/pixel for the coating eccentricity. During the test measurements, small errors could be introduced into the fibre geometry, both in terms of diameters and eccentricity of coating layers. Fibre samples were also measured with a conventional offline instrument. The differences between coating diameter online test measurements and offline measurements were approximately $\pm 1 \mu\text{m}$, and difference in the changes of eccentricity were under 0.1 μm .

The uncertainty components of the measurement of inner diameter and concentricity are listed in table 1.1. The measured parameter is the position of a preselected interference peak, which is calculated from the image using the pixel pitch of the sensor and the distance front the fibre to the sensor.

Table 1.1. Main identified measurement uncertainty components

Source component	Value	Distribution	Standard uncertainty of scattering feature angle
Fibre to sensor distance error	30 μm	Normal	0.014° (symmetrical)
Measurement beam to sensor alignment error	0.3°	Normal	0.0003° (asymmetrical)

Resolution of sensor	7.04 μm	Rectangular	0.005°
Repeatability	0.2°	Normal	0.2°
Combined standard uncertainty			0.201°

The 0.2° uncertainty in the angle of the scattering feature corresponds to the coating diameter uncertainty of 1.8 μm if effects are symmetrical and to 0.1 μm of eccentricity if the effects are asymmetrical. **4.1.2 Measurement of optical dispersion**

The aim of this work was to develop non-destructive and novel methods to measure dispersion and group velocities in optical fibres. The target was to measure optical dispersion with a relative uncertainty of 1×10^{-3} for dispersion slope and zero dispersion wavelength for 100 m of silica fibre.

This chapter describes the new developed methods, one of which is utilizing a tuneable pulsed light source and timestamping electronics. The other is a SEA TADPOLE type white-light spatial-spectral interferometer, customised for characterising optical fibres.

The first setup uses White Rabbit (WR) technique, and in its core principle is a time of flight measurement at different central wavelengths of the optical pulses. The experimental setup of measuring the fibre dispersion is a custom made in collaboration between VTT and Aalto. The first version of the setup employed a frequency comb with a monochromator as a source, which was implemented with support from CMI. In the final version, the source is replaced with a supercontinuum laser source (L) with a Fabry-Perot interferometer (FPI) to achieve a sufficient collection efficiency. The light from a supercontinuum laser source in the spectral range of 1280 nm to 1680 nm is filtered with a MEMS-based electrically tuneable Fabry-Perot interferometer. The light is coupled into a short fibre (F1) with an off-axis parabolic mirror. The fibre with protective coating is removed, is bent to the extent that a portion of the light travelling in the fibre radiates out through the cladding (bent loss). Most of the light remains in the fibre and will be guided to the fibre spool under the study (FS). After the fibre spool, the light is guided to a short fibre (F2), and a bent loss is introduced again. The light from the bent loss is focused on a fast optical detector (APD) and analysed to calculate the time the light was in the fibre. Schematic of the setup is shown in figure 1.3.

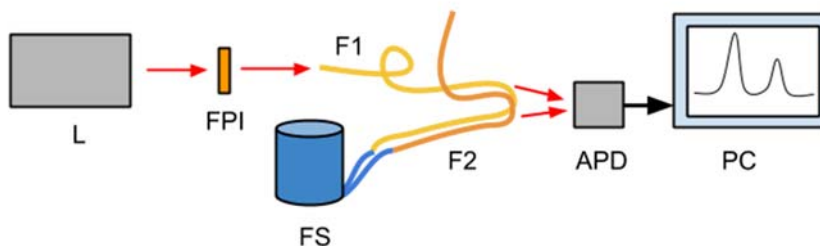


Figure 1.3: The principal layout of the WR measuring setup. L - free space supercontinuum laser, FPI - Fabry-Perot interferometer, F1 - short fibre with an off-axis parabolic mirror, FS - the fibre spool under the study, F2 short fibre. The light from the bent losses from fibres F1 and F2 are focused on a fast optical detector - APD.

The dispersion can be estimated based on the time the pulses with different central wavelengths stored in the fibre. In principle, a fibre of any length can be measured with this method, but characteristics of the optical pulses sent into the fibre and the characteristics of the detector are limiting the minimum length. In addition, to establish a comparison point, a fibre spool of 10 km was chosen provided by METAS, which could also be measured with conventional methods. The estimated relative uncertainty for the measurement of the chromatic dispersion is less than 2% at the 95% of confidence interval.

The second setup uses a SEA TADPOLE technique, which is a variant of spectral interferometry (SI). SI is a linear method for measuring the phase difference of two impulses and it can also be used to measure the response of optical systems. The main principle of spectral interferometry relies on measuring the combined spectrum of an unknown and a reference pulse, where one of them is delayed with respect to the other. This yields an interference in the frequency domain and the spectral phase of the unknown pulse with respect to the reference pulse can be retrieved. One of the variations of SI is spatial-spectral interferometry, which uses non-collinear beams and imaging spectrometer to record a 2D trace. The spectral phase information can be

retrieved from interference fringes perpendicular to the frequency axis, and no spectral resolution is lost during the retrieval. SEA TADPOLE technique uses equal length fibres on the both arms of the interferometer.

The experimental setup for measuring fibre dispersion is based on SEA TADPOLE interferometer and was built by UT. Metroserf provided assistance in estimation of measurement uncertainty. The beam from supercontinuum laser L with spectral range of 428-1088 nm, is expanded with beam expander BE and directed to a fused silica window BS1 to divide the beam into two interferometer arms. In the reference arm the beam is directed with mirror M1 through a second fused silica window BS2, which acts as a dispersion compensation plate. Subsequently the light is directed through a variable delay line D and focused into photonic crystal fibre PCF1 with a parabolic mirror SM1. The beam in measurement arm is directed with mirrors M2, M3, M4 to a focusing mirror with same properties as in reference arm. It focuses the light into the optical system S under investigation (fibre in our case) from where the light is collected with a secondary photonic crystal fibre PCF2. The lengths of PCF1 and PCF2 are equal and thus the dispersion from them is negligible. In the case of ultrabroadband illumination, photonic crystal fibres are required to ensure single-mode operation over the entire spectrum. The output of the fibres is placed on the entrance slit of an imaging spectrometer with a few mm separation, so that light enters the spectrometer under a small angle 2θ perpendicular to the frequency axis ω . The spectrometer consists of a spherical mirror SM2, reflecting half-prism P, cylindrical lens CL, and a CCD camera. A spatial interference pattern on the CCD camera is processed to retrieve the spectral phase and amplitude information of the field correlation function. We use CCD as our detector, which limits our spectral range. Therefore with this system we can only measure in visible and near infrared. The schematic of the setup is shown in figure 1.4.

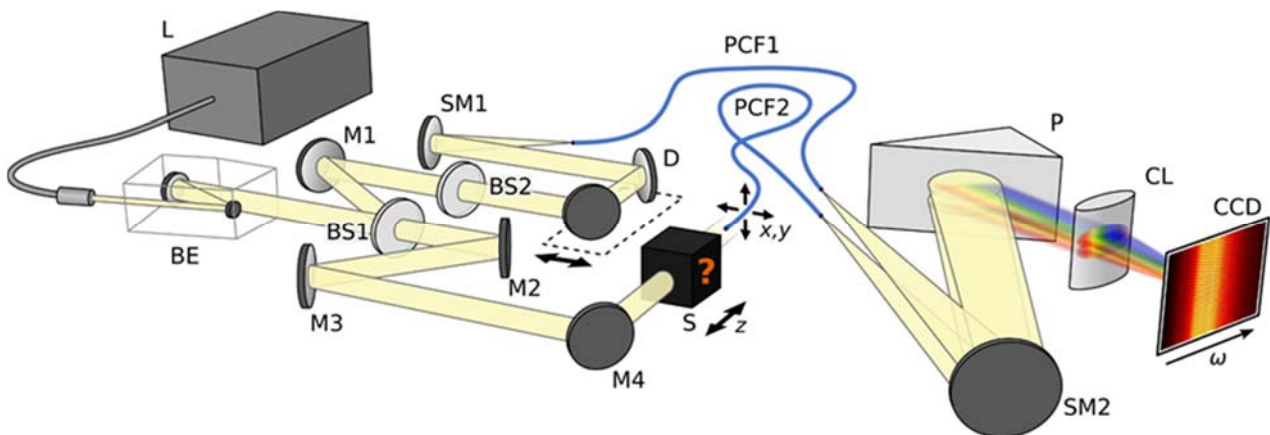


Figure 1.4. Schematic of the SEA TADPOLE setup.

In our case both of parabolic mirrors were changed to lenses in both interferometer arms to simplify system usage when doing empty measurements and fibre dispersion measurements. In the interferometer's measurement arm the location of the focusing lens is for the empty measurement in front of PCF2 and then for the actual fibre dispersion measurement moved before the system S (fibre). The light is directed from the fibre to PCF2 over air. Fused silica rods with known length and dispersion are placed to the reference arm to compensate fibre dispersion and basically weigh the dispersions against each other.

The dispersion can be calculated from the camera image where interference fringes show the spectral phase relation to frequency. By taking into account all the dispersions in the interferometer, one could calculate the dispersion of the unknown fibre as a second derivative of the spectral phase. This method enables to measure fibre dispersion in wide spectral range with single shot measurement.

Proof-of-principle measurements were performed with Thorlabs fibre 630HP, and results were compared with the dispersion curve provided by the manufacturer. The estimated relative uncertainty for the refractive index at 600 nm is 1.5×10^{-3} .

4.1.3 Measurements in high power applications

Components used in high power fibre systems differ significantly from those employed in systems designed for lower average power, e.g. telecommunications and sensing. The focus of this work was an investigation of cladding light in double clad fibre systems, as this parameter is critical for high power operation and is often disregarded. A non-invasive method for cladding light measurement was developed. The needs of the fibre industry and the results achieved were actively discussed between the partners throughout the project. The

experiments performed were designed and agreed between FhG, CSIC and the industrial partners that manufacture fibres (nLIGHT and Oplatek). Measurements were carried out at FhG, nLIGHT and Oplatek supplied double-clad fibres for testing. A Good Practice Guide titled "Guidelines on measurement procedures for high power fibre optics" was written by all project partners involved in high power activities.

Double clad design may hinder optical characterization of fibres or components. While light leaking from the inner signal core can effectively no longer be used in the designated application, it is still guided in the cladding and will thus be measured by power detectors, and this may distort loss measurements. Furthermore, the appropriate definition of cladding light depends on the application at hand. For example, when the interest is to avoid heating up the opto-mechanics on the fibre output end, the amount of high numerical aperture light is of interest. On the other hand, when the interest is estimating the amount of cladding light for subsequent integrated fibre components, the amount of light that is located in the cladding area is required. Origin of the cladding light can be, among other reasons, due to direct coupling, due to incorrect splicing or due to scattering from fibre defects, as illustrated in Figure 1.5.

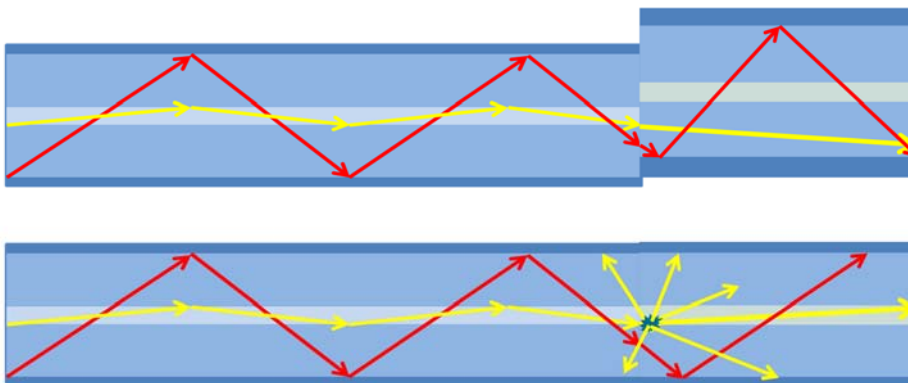


Figure 1.5. Origin of cladding light, due bad splice (offset) above, and due to scattering from a fibre defect (below)

Cladding light differs from the light in the signal core in numerical aperture and near field diameter, it typically cannot be focused as tightly as core light and is probably not fully usable in the desired laser application. However, depending on the measurement setup, in many cases cladding light is included in laser power measurements. It thus leads to a misconception concerning the usable optical power of a fibre laser system. In high power applications, cladding light can also cause thermal issues by heating up absorbing material that is in direct contact with cladding, or the optomechanical components, e.g. lens mounts.

Commonly employed methods for evaluation of the cladding light content in double clad systems are prone to very high errors. One method is to image the fibre facet onto the aperture in front of the power meter to measure the core light only, and comparing it to the measurement without the aperture. However, the diameter of the aperture is not well defined, and furthermore, the cladding light has an overlap with the signal core. A different method would be to measure light in the far field from a collimated beam, but that equates to measurement of high-NA light, which leads to underestimation of the cladding light content. A third method is based on measurement of power output when cladding light strippers are applied (CLS). This method is invasive, and dependent on the efficiency of the CLS. For high power applications, thermal issues may also become relevant.

To address these problems, the "constant intensity extrapolation" (CIE) method was developed. CIE is based on the assumption that the average intensity in the fibre cladding is nearly constant. This is given in the cladding area for any fibre with a high number of cladding modes, which is true for nearly every double-clad fibre. If a centered aperture is gradually closed within the area of constant intensity, a plot of aperture area vs. measured power yields a linear relation, as illustrated in figure 1.6.

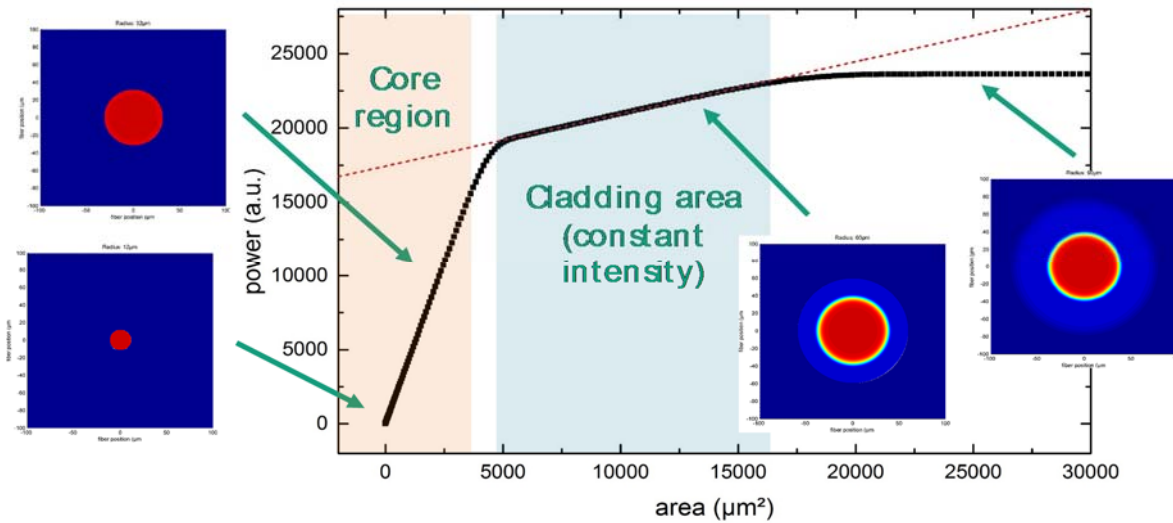


Figure 1.6. Plot of aperture area vs. measured power. A linear relation can be easily identified in the cladding region of constant intensity (example: super-gaussian core- and cladding intensity profiles). Beam profiles as viewed through the aperture are depicted for the respective regions.

A setup for non-invasive measurement of cladding light in double clad fibres was built, as depicted in Figure 1.7. This setup also allows for measurement at high average power, employing a high power signal laser as light source. The setup consists of an input coupling for a test laser into the fibre under test. In the case of high power test operation, endcaps can be added to the fibre facets. At the output, the fibre facet is imaged onto the plane of a variable aperture (iris diaphragm) and the power behind that aperture is measured by a power meter.

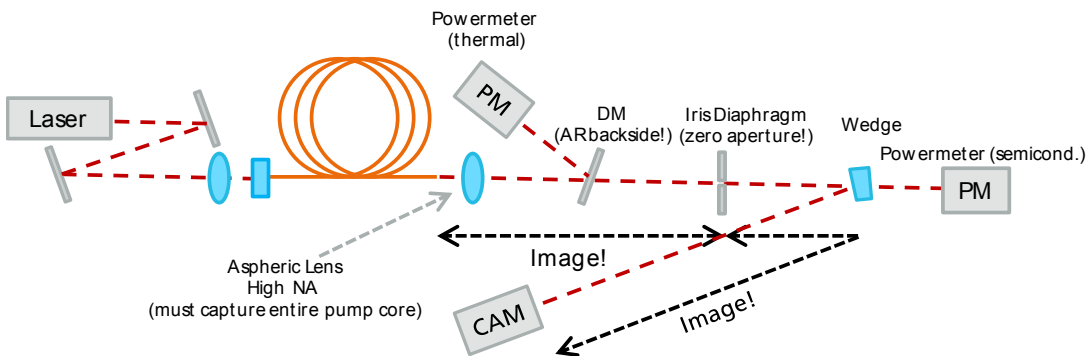


Figure 1.7. Setup for measurement of cladding light content in double clad fibres at high average power. The fibre under test is shown in orange.

Due to the linear fitting, and since the core light power can be directly read from the linear fit’s y-axis intersection, increasing the number of data points available for fitting directly improves the accuracy of the measurement. In the performed test measurements, the relative uncertainty of core light content was below 4.2 %, which is estimated from the accuracy of the power meter and aperture diameter measurements. A repeatability of $\pm 0.5 \%$ (absolute, $< 3 \%$ relative) for the core light fraction was shown when repeating the same measurement.

A theoretical comparison between the CIE method and the measurement of core light by closing an aperture has been done for different experimental conditions. As mentioned before the definition of the clipping point for the aperture diameter proved to be the factor inducing the highest error in the latter method. Depending on the fibre geometry under investigation, the CIE method outperformed the “core-transmission-only” method significantly, with the difference increasing with the signal core diameter (due to cladding light in the signal core area).

4.1.4 Summary of key research outputs and conclusions

The project provided non-destructive and novel methods (offline) to measure dispersion and group velocities in optical fibres, measurement procedures for high power fibre optics, and online techniques for dimensional measurement of optical fibres.

Two novel set-ups for dispersion measurement of optical fibres were built. One utilises a supercontinuum laser, a MEMS based electrically tuneable Fabry-Perot interferometer for wavelength selection and White Rabbit technique for time synchronisation. This setup allows measurements of fibres of arbitrary length, including very short ones. The other is based on a SEA TADPOLE type white light spatial-spectral interferometer. The reached estimated uncertainty was 1.5×10^{-3} .

A setup for the evaluation of cladding light content at up to 400 W was successfully implemented and tested, reaching the target accuracy of $\pm 5\%$ and allowing for the cladding light measurement in multi-clad fibre geometries.

A method based on the analysis of a laser scattering pattern, as the fibre is illuminated transversely during the drawing process was developed for real-time dimensional characterization of coating layers of an optical fibre. The method was implemented and tested in a prototype instrument in a production environment. The uncertainty for the coating diameter measurement of the tested fibre was $1.8 \mu\text{m}$ and the uncertainty for the coating eccentricity was $0.1 \mu\text{m}$.

4.2 Metrology for improved traceability of fibre-optic measuring instruments

This objective included the development of several calibration techniques and artefacts that were characterised and successfully validated to improve traceability of fibre-optic measurements.

4.2.1 Traceable Encircled Angular Flux (EAF) measurements

Traceable measurements of the modal distribution in multimode fibres have become important, since correct measurements of quantities like the insertion loss or the bandwidth strongly depend on how different guided modes are populated in the fibre. Several metrics for the modal distribution like the Encircled Flux (EF) already exist and are fully traceable but are not applicable to many type of fibres like step index large core or plastic optical fibres. The EAF was proposed to overcome this issue. This metric is based on the evaluation of the far field intensity pattern observed at the output of the fibre, and allows taking into account possible radial asymmetries in the modal distribution pattern. First commercially available systems for EAF measurements exist, but the necessary traceability was still missing.

A fully traceable EAF measuring systems was developed by METAS, as shown in Figure 2.1. It consists in 2048 x 2048 pixels CMOS camera with a pixel size of 6.5 μm , which is placed at a distance R of the fibre under test. The system is fitted with a high resolution $XY\theta\varphi$ stage to control the correct positioning of the fibre. A Labview data analysis software was developed for the control of the system and for the online computing of the EAF, based on the measured far field intensity profile.

A detailed measurement uncertainty budget was established by evaluating all relevant factors of influence. The linearity and uniformity of the CMOS camera were calibrated using dedicated methods, traceable to a series of linearity standards (reference detectors) and to a reference uniform illumination source. The calibration of the fibre to camera distance R was performed optically, using a traceable high resolution optical Low Coherence Reflectometer (OLCR) with a measurement uncertainty of $u_R = 20 \mu\text{m}$ ($k=2$).

Specific algorithms to compensate the refraction of the beam through the camera entrance window were implemented.

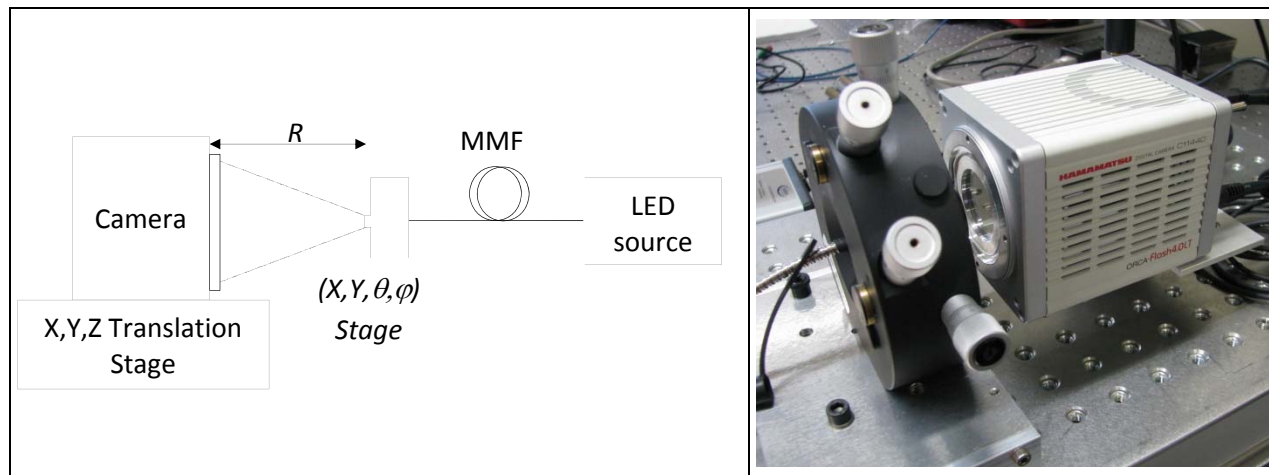


Figure 2.1. Measuring system for traceable EAF measurements. A CMOS camera collects the far-field intensity profile at the output of the multimode fibre under test (MMF), which is placed in front of the camera at a fixed known distance R .

Based on these evaluations, the influence of the different factors was propagated to the EAF measurement numerically, using the same Labview data analysis software. The detailed measurement uncertainty budget is shown in Figure. 2.2 for the EAF value where the expected measurement uncertainty is the largest.

Uncertainty component	Source of uncertainty	Value	Distribution	Standard uncertainty
$u_{EAF_{Unif}}$	Uniformity of CMOS camera	0.0012	rectangular	0.0004
$u_{EAF_{Lin}}$	Non-linearity of CMOS camera	0.0005	rectangular	0.0002
$u_{EAF_{\Delta R}}$	Fibre to camera distance	0.0015	rectangular	0.0005
u_{EAF_W}	Correction of the refraction through camera entrance window	0.0013	rectangular	0.0004
$u_{EAF_{\Delta Z}}$	Pixel size and limit of resolution	0.0002	rectangular	0.0000
$u_{EAF_{Rep}}$	Repeatability	0.0001	normal	0.0000
$u_{EAF_{CW}}$	Uncertainty arising from the non-ideal correction of the refraction through the CMOS chip window	0.009	rectangular	0.003
Expanded combined standard uncertainty (k=2)		U_{EAF}		0.005

Figure 2.2. Uncertainty budget of the METAS EAF measuring system, calculated for the EAF value having the largest expected uncertainty, in case of a GI 50/125 fibre.

The achieved level of uncertainty is compatible with the expected requirements arising from the EAF templates (limit values), as currently under discussion within the IEC TC86/SC86B/WG4.

A second independent EAF measuring system, also based on the analysis of the far field intensity profile, was developed by Arden and is shown in Figure 2.3. This system uses a larger size camera and different image processing algorithms and was built to transpose the specifications of the reference EAF system developed by METAS into a more industrial product. The collaboration between Arden and METAS made the inter-comparison measurements between two independent setups possible and thus to establish their traceability.

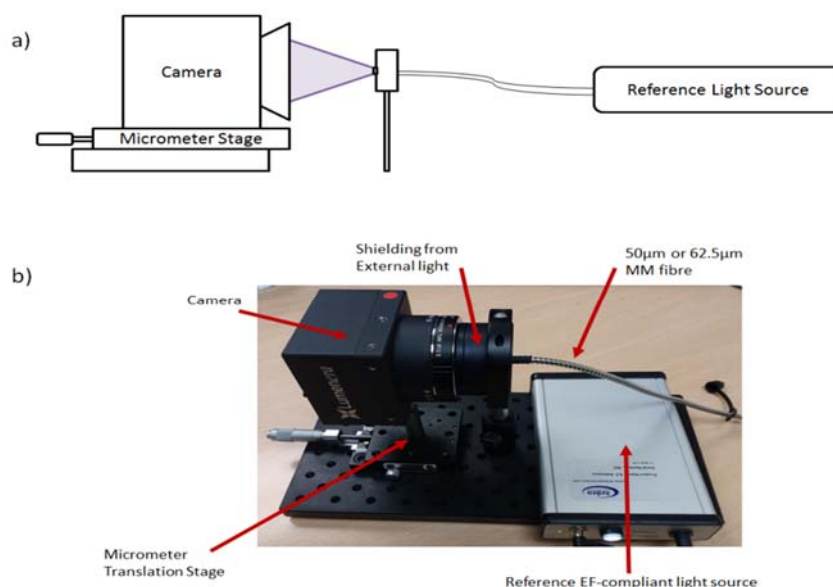


Figure 2.3. Arden instrument for the measurement of the EAF. (a): Sketch of the mounting; the fibre is fixed at a known distance in front of the camera; the distance can be tuned depending on the numerical aperture of the fibre under test. (b): Picture of the system; the red arrows show the main components.

The Arden instrument was calibrated using the same techniques and standards as for the METAS system.

A crossed validation of these two systems was successfully carried out by inter-comparison, based on the measurement of a series of Graded-Index (GI) and of Step-Index (SI) multimode fibres with different numerical apertures and core diameters using the two different systems. These comparisons demonstrated the good comparability of the two instruments, within the estimated uncertainty for the comparison, as show in Figure 2.4, where the deviation between the EAF measurements performed with the Arden and with the METAS systems is shown, in case of the measurement of a 100 μm core SI fibre. The expanded standard measurement uncertainty for the intercomparison was of $U_{\Delta EAF} = 0.005$.

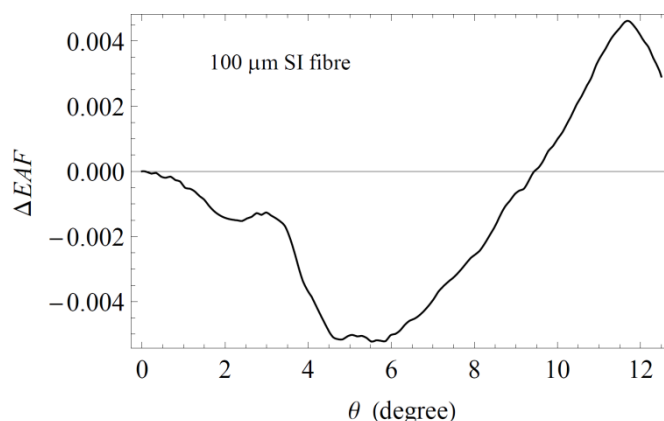


Figure 2.4. Deviation between the EAF measurements performed with the Arden instrument and with the METAS reference system systems. Both results are in a very good agreement, within the estimated expanded standard uncertainty for the comparison, which is of $U_{\Delta EAF} = 0.007$.

The traceable EAF measuring systems validated in the frame of this project have the potential to enable better and comparable measurement of quantities like losses and bandwidth in SI multimode fibre systems. This will also directly contribute to the further improvement of relevant normative documents, as those currently under development within the IEC. Contacts have been taken with the relevant normative bodies and more extended collaborations will be promoted in the future, based on the achieved results.

Different models were developed, jointly by JCM and by METAS to simulate the modal distribution in multimode fibres and to simulate excitation of these modes by a focused beam, using finite-element methods (FEM). The interfaces and software were successfully tested for the estimation of the coupling efficiency between two fibres by calculating the overlap integrals. Improvements of the finite element method for finding modes localized to specific regions in the geometrical setup have been made available in the development version V3.6.1A of the JCMWave software. These results pave the way to a possible determination of EAF templates, based on FEM simulations to ensure, for example, repeatable power and loss measurements.

4.2.2 Traceable artefacts for the calibration of the distance scale of high resolution optical reflectometers

The calibration of the distance scale of high resolution optical reflectometers like OTDR (Optical Time Domain Reflectometers) and OLCR (Optical Low Coherence Reflectometers) requires traceable artefacts allowing generating evenly spaced reflective at the required level of accuracy, which didn't exist until now. The development of the necessary standards to solve these issues was addressed in this project.

An artefact for the calibration of the distance scale of high resolution OTDR was successfully developed. It is based on a singlemode fibre recirculating delay line with a length of (0.888 ± 0.001) m as shown in Figure 2.5, and generates a train of pulses with a distance separation given by the half optical length of the delay line when interrogated with an OTDR. The artefact was calibrated using classical time of flight techniques.

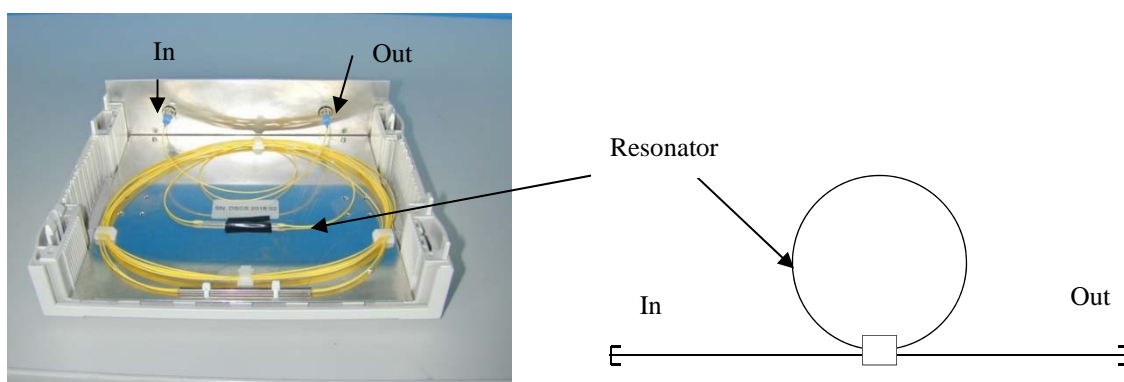


Figure 2.5. Recirculating delay line to be used as artefact for the calibration of the distance scale of OTDR.

To demonstrate the applicability of this artefact, a validation measurement was carried out with a commercially available photon counting OTDR, providing a spatial resolution of 0.2 m with a pulse width of 2 ns. The result is shown in Figure 2.6. The first peak corresponds to the fibre lead connecting the OTDR to the OTDR, whose length is of 0.507 m. The next peak is produced by the first reflection of the OTDR pulse to the end connector of the artefact. The successive peaks are generated by the recirculating delay line itself. The measured spacing is of $\Delta L = (0.882 \pm 0.029)$ m and is in a very good agreement with the calibrated value of (0.888 ± 0.001) m.

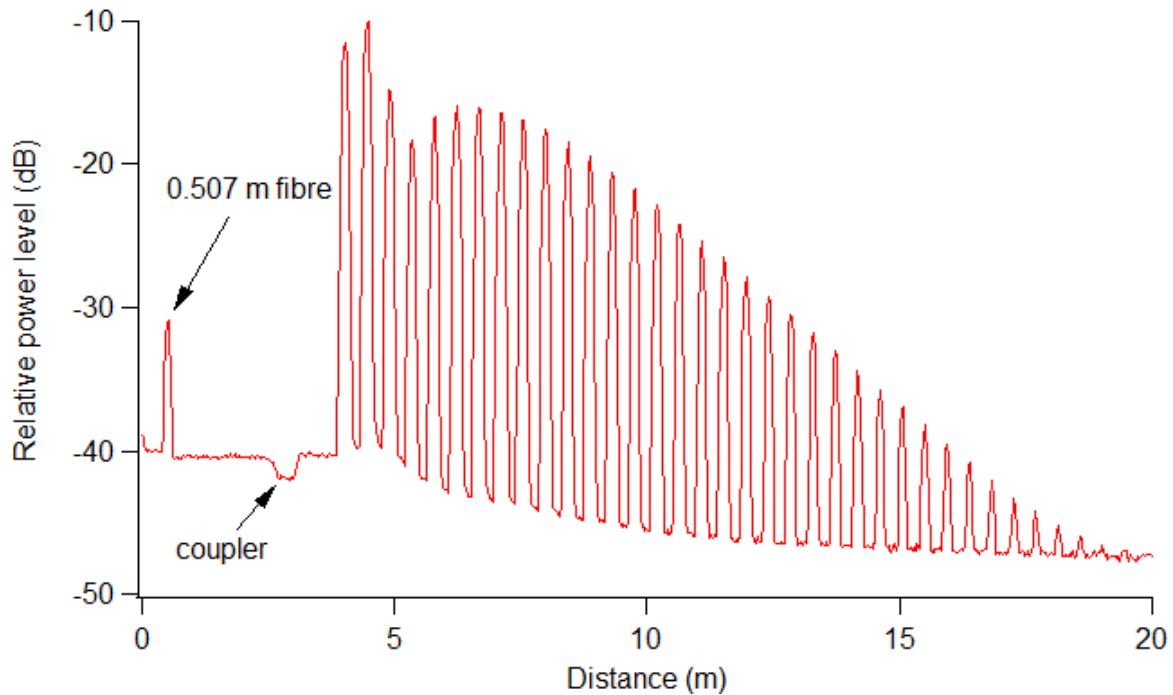


Figure 2.6. Measurement of the calibration artefact with a commercially available photon counting OTDR. The evenly distributed reflection events produced by the artefact are clearly visible and can be used for the calibration of the distance scale of the instrument.

Thanks to the very small size, this artefact is also ideally suited for the characterization of the limit of resolution of high resolution OTDR. It is now available within the project partners for inter-comparison measurements.

An artefact for the calibration of the distance scale of Optical low coherence reflectometers (OLCR) was also successfully developed. It consists of a fibre-coupled, air-spaced asymmetrical Fabry-Perot resonator, which consists in a singlemode fibre pigtail with a 50 % reflective coating placed at a distance L_{ref} of a 100 % reflecting ferrule, as shown in Figure 2.7 (left).

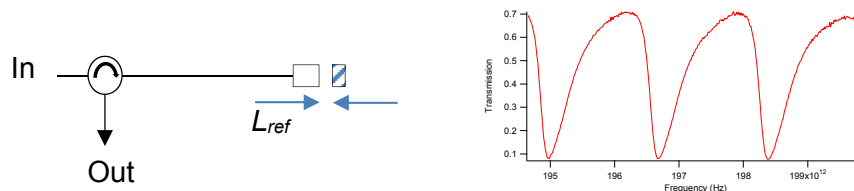


Figure 2.7. Left: Fibre-coupled air-spaced resonator built using a coated bare fibre and a mirror separated by a distance L_{ref} . Right: spectral reflection of the resonator.

The distance L_{ref} between successive reflective events was calibrated by measuring the Free Spectral Range (FSR) of the resonator using a tuneable extended cavity laser traceable to a reference wavemeter, and by calculating L_{ref} according to $L_{ref} = c/(2 \cdot FSR)$, where c is the speed of light in vacuum. The reflection spectrum of the resonator is shown in Figure 2.7 (right). This led to a value of $L_{ref} = (88 \pm 1)$ μm .

The artefact was tested by comparison to a reference OLCR, with a spatial resolution of 10 μm . The measured reflection pattern is shown in Figure 2.8. The measured peak separation was of $(86 \pm 5) \mu\text{m}$, which is in a very good agreement with the calibrated values, well within the measurement uncertainty of the comparison.

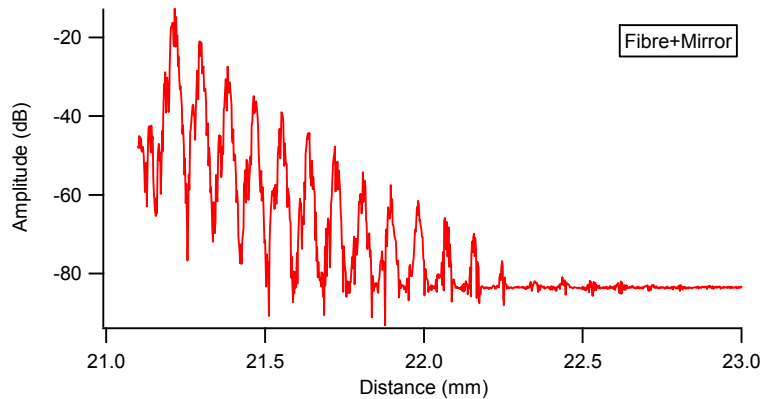


Figure 2.8. Measurement of the artefact with a reference OLCR. The measured peak position and spacing are in a very good agreement with the calibrated values, well within the measurement uncertainty.

This artefact is well suited for the calibration of commercially available OLCR and allows the calibration of the distance scale of the instrument and the evaluation of the spatial resolution of such instruments. It is available within the project partners for inter-comparison measurements.

4.2.3 Traceable artefacts for the calibration of the attenuation scale of multimode Optical Time Domain Reflectometers (OTDR)

Attenuation measurements in multimode fibre-based components and systems may strongly depend on the modal distribution of the light propagating in the fibre. For that reason a careful control of the modal distribution is necessary to overcome this issue. The same problem arises when measuring losses using Optical Time Domain Reflectometers (OTDR), and the correct calibration of the attenuation scale of these instruments requires calibration artefacts and references taking into account the modal distribution.

METAS developed for that purpose two attenuation reference fibres with controlled modal distribution, which consist of a spool of a 50 μm or of 62.5 μm multimode fibre of a length of about 2 km, which is connected to a mode conditioner as shown in Figure 2.9. The mode conditioner was chosen in order to generate a reference modal distribution at the input of the fibre spool, conform to the IEC 61280-4-1 standard, and meantime to keep a more overfilled distribution of the backscattered signal.

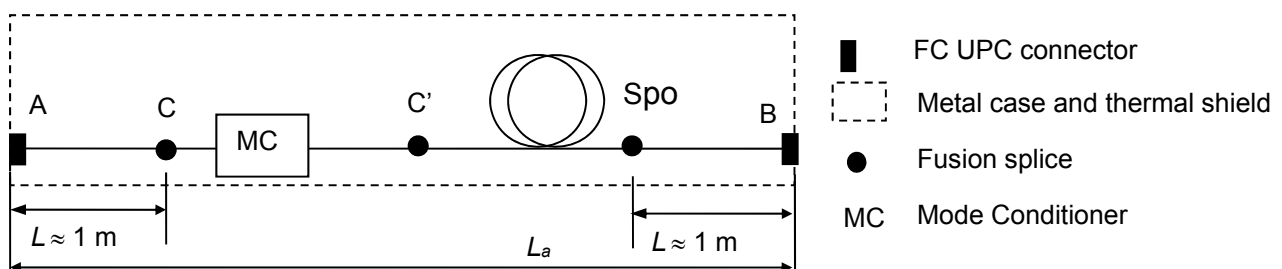


Figure 2.9. Inner structure of the multimode attenuation reference fibre with controlled modal distribution.

The fibre was conditioned on a reel in a special way to minimise possible micro- and macro-bending effects. The artefact was mounted in a thermally protected housing for better long term stability. The inner of the fully built artefact is shown in Fig. 10 (left). The spectral attenuation of the artefact was calibrated using an especially developed cut-back method with controlled modal distribution, which is traceable to the power and wavelength scales maintained at METAS. The typical results are shown in Figure 2.10 (right). The uncertainty of the measured total attenuations was of about 0.03 dB in the whole spectral domain, ranging from 750 nm to 1400 nm.

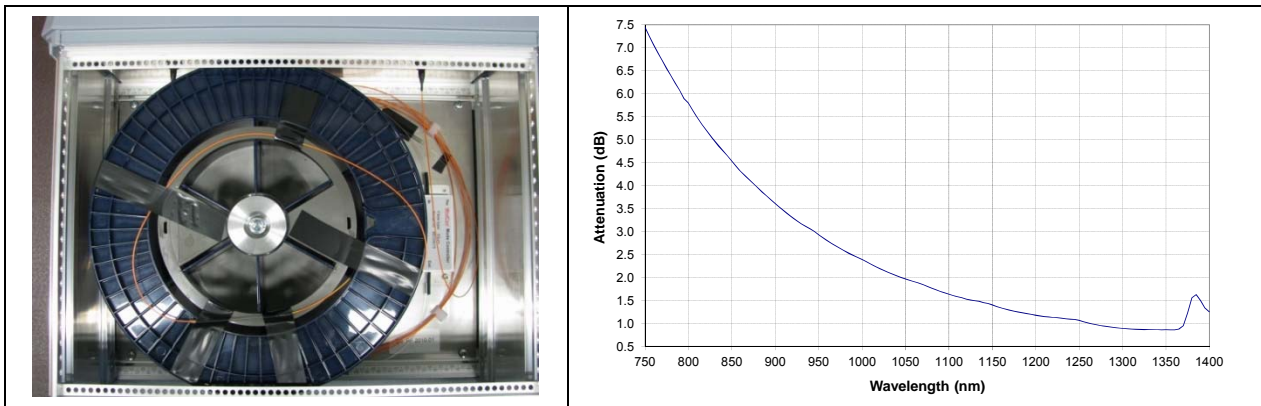


Figure 2.10(left): Inner structure of the calibration artefact with the fibre spool and the mode conditioner mounted in a metal case. Right: Spectral attenuation of the 2 km long 50 μm fibre artefact measured from 750 nm to 1400 nm.

These artefacts are ideally suited for the calibration of the attenuation scale of multimode optical time domain reflectometers (OTDR). This was demonstrated by performing the calibration of the attenuation scale of a high performance 62.5 μm multimode OTDR. For that purpose the setup shown in Figure 2.11 was used. A tuneable attenuator and a series of lead-in fibres of different lengths were placed in front of the artefact, allowing performing the calibration at several power levels and locations all along the distance scale of the instrument. A reference attenuation value A_{ref} was generated by selecting a given length of fibre in the artefact, starting at a specific location L along the fibre. The reference attenuation was then measured with the OTDR and the relative deviation of the loss scale $\Delta A = A_{OTDR} - A_{ref}$ was determined. This measurement was repeated at different locations L and also for different values of the relative power level F , which was referenced to the saturation (clipping) level of the instrument.

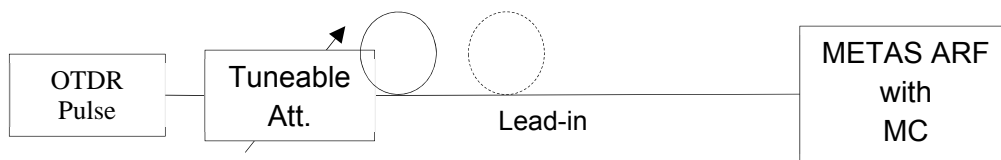


Figure 2.11. Measurement setup used for the calibration of the attenuation scale of MM OTDR.

The results of the calibration are shown in Figure 2.12, where the deviation of the attenuation scale is shown as a function of the distance L (left) and of the relative power level F , referenced to the clipping level of the OTDR (right).

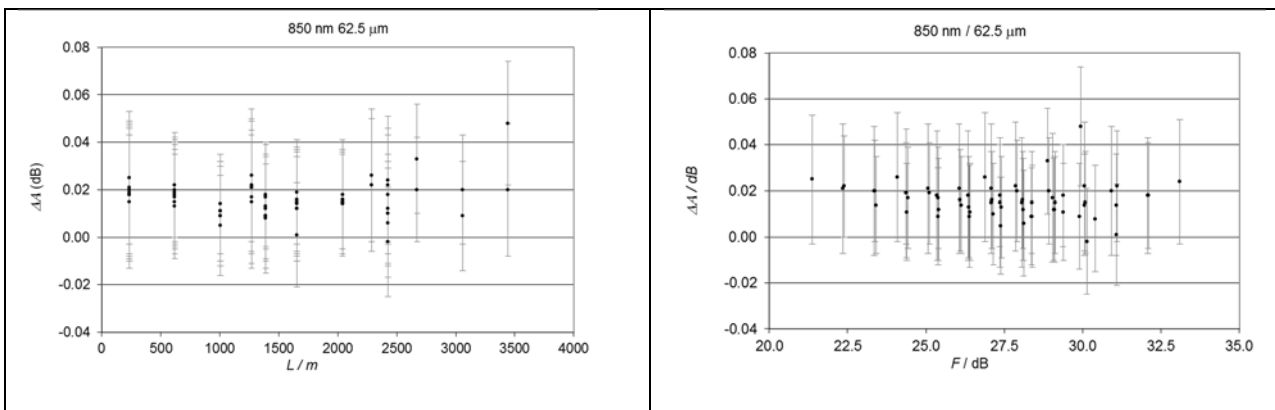


Figure 2.12. Deviation of the attenuation scale of the high-performance OTDR as a function of the position L (left) and of the relative power level F (right).

Both results showed a very small deviation ΔA , compatible with a zero value, within the measurement uncertainty, which was of $U = 0.03$ dB for all measurement points. The achieved results demonstrate that these new artefacts allow the calibration of the attenuation scale of multimode OTDR in an absolute way with a very low measurement uncertainty, which was not the case until now.

The two artefacts were sent to one of the leading company fabricating OTDR for testing. The onsite calibration of two different high-performances OTDR was carried out and the results of the calibration performed at 850 nm on the 50 μm artefact are presented in Figure 2.13. They show very good results, comparable to those obtained with the METAS reference OTDR, confirming the metrological interest of these artefacts.

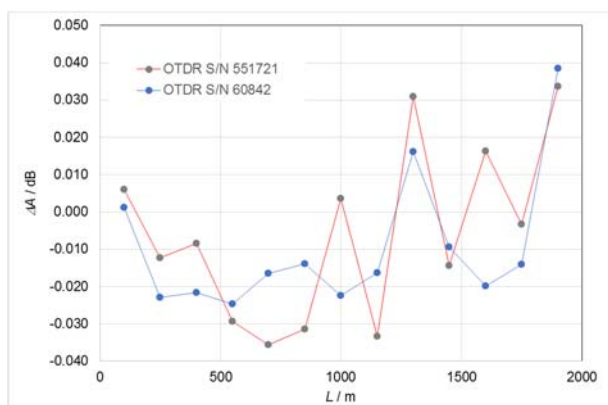


Figure 2.13. Deviation of the attenuation scale of two different high-performances OTDR measured with an industry partner. Both results show similar behaviours as those observed with the METAS reference OTDR.

The integration of such a procedure in the relevant international standard IEC 61746-2, “Calibration of optical time-domain reflectometers (OTDR)- Part 2: OTDR for multimode fibres” would bring the advantage of offering a very simple method for the high accuracy calibration of the absolute attenuation scale in a simple way, which does not exist at the moment. On the other hand, implementing this new method in the standard may have important consequences to the industry, especially regarding how the instrument specifications should be adapted and presented to the customers. Further discussions need to be carried out with the industry and within the IEC TC-86 WG4 to find the best way of optimally using these new calibration standards. This artefact will be used to offer new calibration services at METAS and is available within the project partners for inter-comparison measurements.

4.2.4 Reference systems and calibration techniques for OTDR distributed optical-fibre sensors

New calibration techniques and performance enhancement strategies for distributed and quasi-distributed fibre sensors were developed. Regarding sensor calibration, the following calibration techniques were established:

- Fibre Bragg grating interrogator calibration based on the direct comparison between the wavelength measurements of the interrogator under test and a calibrated wavemeter, while analyzing a simulated tunable symmetric Bragg grating composed of a tunable filter and a fibre mirror. This method presents an uncertainty of 1.1 pm, limited by the spectral width of the tunable filter and the wavelength stability of filter and wavemeter.
- Fibre Bragg grating interrogator calibration based on measuring multiple reference absorption lines of calibrated absorption gas cells covering the operating wavelength range of modern commercial FBG interrogators. This second method presents an even better uncertainty (down to 0.6 pm), providing a more sensitive calibration of high-accuracy Bragg grating interrogators and enabling wavelength-dependent correction constants. However, despite providing a more accurate characterization of the devices, the second method is only applicable to commercial systems equipped with software post-processing tools that are capable of characterizing absorption lines.
- Simultaneous resolution and temperature calibration of distributed fibre sensors, based on the combination of a first liquid-filled receptacle with varying temperature where a long fibre span is submerged, and a second receptacle where multiple spools of progressively increasing length are introduced.

These techniques were incorporated to the catalogue of CSIC calibration services, which are available to all project partners involved in distributed sensing (WWU, METAS and NPL).

Regarding sensor enhancement, two novel schemes have been demonstrated: an OTDR with a photonic differentiation detector which determines both phase and amplitude of the backscattered pulse, providing high resolution and sensitivity temperature measurements while circumventing the need of a reference state; and a coherent-OTDR for distributed vibration measurement based on chirped pulses and instantaneous frequency analysis which provide single pulse characterization with high resolution and sensibility.

These sensor enhancements are proprietary results, protected through patent applications P201530793ES and P201531736ES, but all non-confidential information and knowledge associated to both inventions is available to the partners of the consortium.

Furthermore, a novel surveillance system aimed at the detection and classification of threats in the vicinity of a long gas pipeline based on phase-sensitive optical time domain reflectometry (ϕ -OTDR) technology was developed. Contextual information at the feature level was incorporated and a system combination strategy for pattern classification was applied. The contextual information at the feature level is based on the tandem approach (using feature representations produced by discriminatively-trained multi-layer perceptrons) by employing feature vectors that spread different temporal contexts. The system combination strategy is based on a posterior combination of likelihoods computed from different pattern classification processes. In comparison with a previous system based on the same rigorous experimental setup, the results show that the system combination from the contextual feature information improves the results for each individual class in both operational modes, as well as the overall classification accuracy, with statistically-significant improvements. On-line and final blind field test results were conducted on two different pipeline sections: one close to the sensor position, and the other 35 km away from it. Results of machine and activity identification mode showed that about 46% of the times the machine, the activity or both were correctly identified. For the threat detection mode, 8 out of 10 threats were correctly detected, with 1 false alarm.

4.2.5 Absolute Primary Standard Radiometer for optical fibre power measurement

A novel Absolute Primary Standard Radiometer for optical fibre power measurement based on a planar cryogenic bolometer chip (PCBC) was. The PCBC chip has been developed by NIST and is based on a circular 5.5 mm diameter silicon substrate with a forest of carbon nanotubes (CNT) grown on top of it that absorbs 99.997% of the impinging light. The chip contains also a tungsten heater, an Nb transition edge sensor (TES) to measure temperature variations around the working point temperature of about 7.5 K and a heat link optimized for chip operation at about 100 μ W power levels.

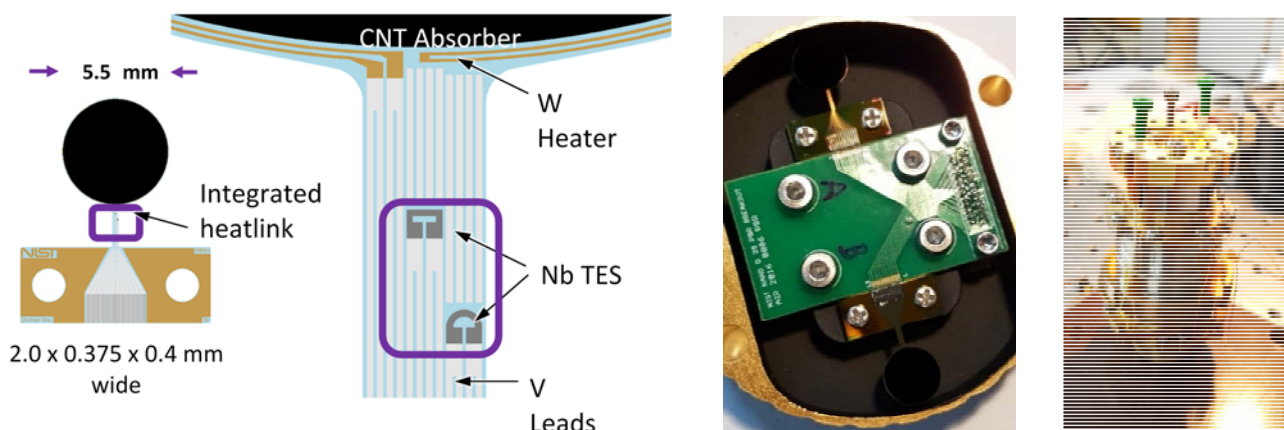


Figure 2.14. Carbon nanotube bolometer chip (courtesy of Malcolm White, NIST). In the middle the chip holder and to the right the reference block with the optical fibre end.

The chip is placed inside a fast cooling low vibration mechanical cooled cryostat. An optical fibre is passed through vacuum feedthrough inside the cryostat and illuminates the PCBC. The end of the fibre is placed at about half of a millimetre distance to the chip so that the output optical radiation underfills the chip. The other end of the fibre is spliced to a pigtailed a FC/PC connector.

Method

An attenuated fibre-coupled laser diode is connected to the input of the MEMS optical switch developed by METAS. METAS has the know-how in building and characterisation of such devices. One of the optical switch's output (Ch2) is connected to the new primary standard while the other output (Ch1) is connected to the CMI InGaAs based power meter that has been calibrated in free beam configuration and is traceable to the CMI primary standard for optical radiometry: the CMI cryogenic radiometer (CR). The PCBC chip is placed on top of a reference block that is actively kept at a stable temperature (about 7K) by a PID control.

The optical switch unit developed at METAS consists in a SERCALO singlemode fibre-coupled 1x2 MEMS switch, which is fitted with a FC APC wide key connector at the IN port and with two pigtailed with FC PC wide key connectors at the OUT1 and OUT2 ports. The internal structure of the unit and its realization are shown in Figure 2.15. The fibre is a standard G.652.D singlemode fibre.

An Arduino-based controller allows driving the switch either with a USB interface using a dedicated Labview driver or with an external TTL trigger signal. The splitting ratio between the two outputs $C_{21} = P_{out2} / P_{out1}$ was calibrated at a wavelength of $\lambda = 1550$ nm and was found to be of $C_{21} = 1.0116 \pm 0.0006$.

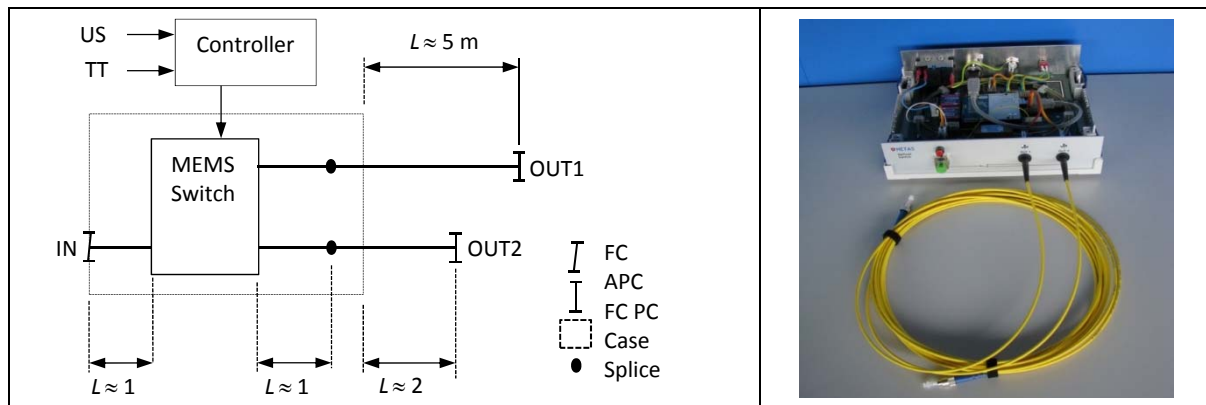


Figure 2.15. To the left the chip holder; to the right the reference block with the optical fibre end.

The reference block PID is realized by a current source that provides the current to the reference block heater and a DC resistance bridge to read the resistance of a CERNOX cryogenic temperature sensor in thermal contact with the reference block. The controlling software provides the PID functionality to keep the temperature of the reference block with a stability better than 50 μ K. The optical power measurement is performed with a static substitution procedure that consists in illuminating the PCBC, measuring the resistance of chip TES sensor by a high precision DC resistance bridge and then replacing the optical illumination with the electrical heating dissipated by the chip W heater and generated by a current source in order to obtain the same chip temperature. The optical measurement is surrounded by an electrical power 250 nW lower (electrical low) and one electrical power 250 nW higher (electrical high). The optical power is then calculated by a linear approximation based on these two applied electrical power levels. The electrical power is measured by a digital voltmeter (DVM) that reads the voltage across a 1K Ohm standard resistor connected in series to the current source and by a second DVM reading the voltage across the chip heater.

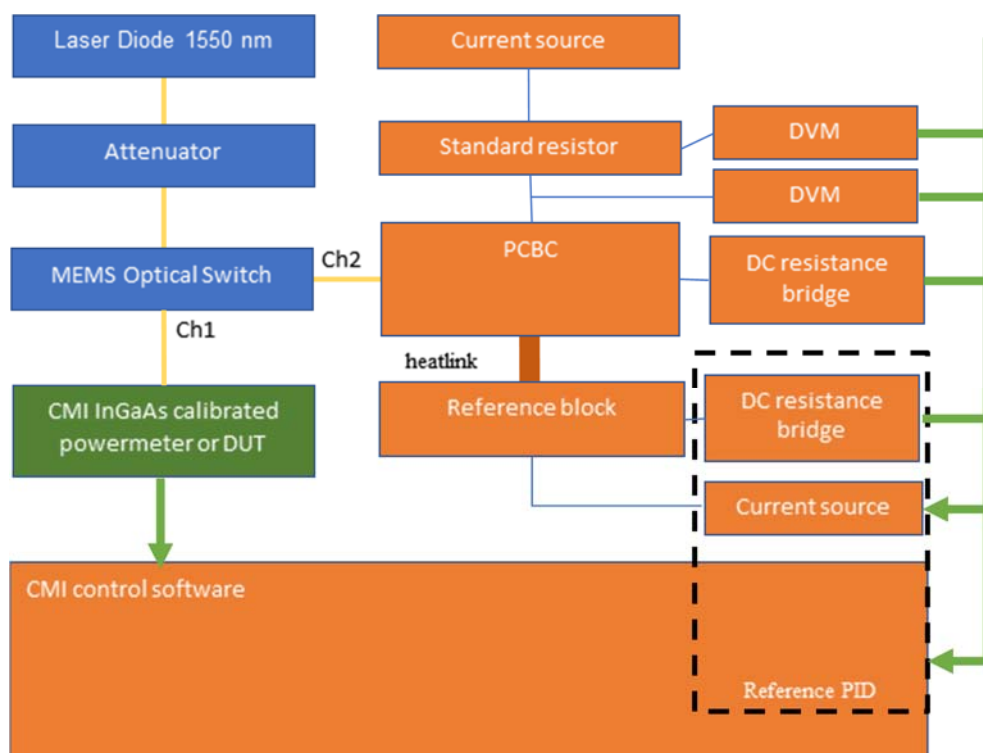


Figure 2.16. Configuration of the optical (blue colour) and primary standard (orange) sub-systems.

The reference block PID is realized by a current source that provides the current to the reference block heater and a DC resistance bridge to read the resistance of a CERNOX cryogenic temperature sensor in thermal contact with the reference block. The controlling software provides the PID functionality to keep the temperature of the reference block with a stability better than 50 μK . The optical power measurement is performed with a static substitution procedure that consists in illuminating the PCBC, measuring the resistance of chip TES sensor by a high precision DC resistance bridge and then replacing the optical illumination with the electrical heating dissipated by the chip W heater and generated by a current source in order to obtain the same chip temperature. The optical measurement is surrounded by an electrical power 250 nW lower (electrical low) and one electrical power 250 nW higher (electrical high). The optical power is then calculated by a linear approximation based on these two applied electrical power levels. The electrical power is measured by a digital voltmeter (DVM) that reads the voltage across a 1K Ohm standard resistor connected in series to the current source and by a second DVM reading the voltage across the chip heater.

Switching ratio measurement

The MEMS-based fibre coupled optical switch developed by METAS it is used to route the optical signal either to the calibrated power meter (fibre end 1 in Figure 2.172.17) or to the PCBC (fibre end 2). Its main advantage is the high stability of its switching ratio. The measurement is performed placing one detector on the DUT fibre end (1) and the other on the fibre end placed at the bolometer end (2) to take in account all the loss introduced by the fibre connector FC by the fibre splicing and by the fibre used inside the cryostation.

The switching ratio measured at 1550 nm between the fibre end 1 and 2 was measured 12 times giving an average switching ratio $R_{12} = 1.1146$ with 0.23 % standard deviation of the mean.

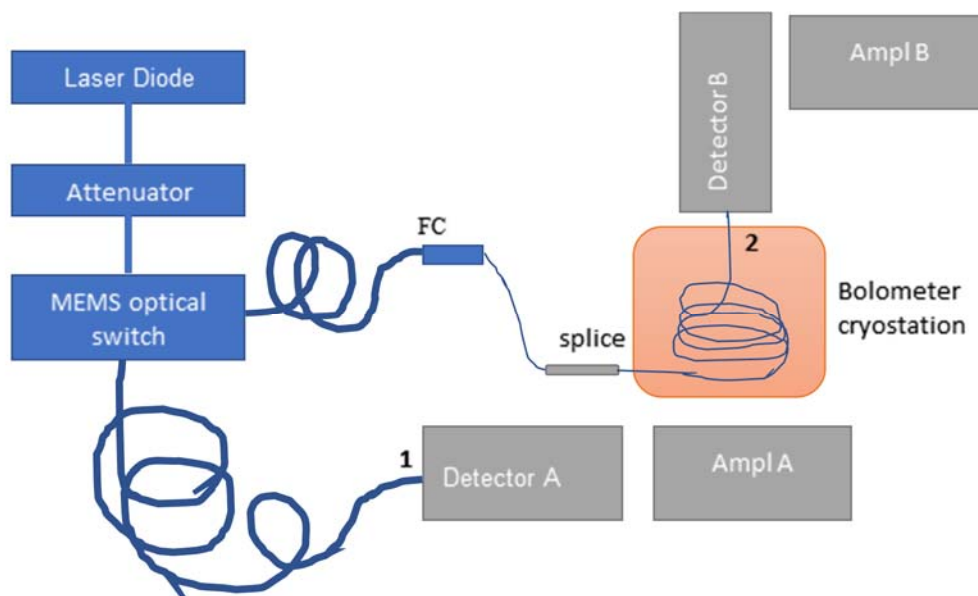


Figure 2.17. Measurement schema of the switching ratio.

PCBC Sensitivity & Noise

The relation between the input power and the PCBC TES temperature (thermal link calibration) was measured around the working point to assess the sensitivity and noise sensitivity of the system. The measurement is performed automatically using a set of electrical power levels. At each power level the software routine waits until the chip temperature reaches stability and records the final temperature.

The temperature to power sensitivity calculated as the slope of the data is 21.2 K/mW. Given that the thermal noise has been measured to be 200 μ K the noise of the system is about 9 nW.

Traceability of the fibre-coupled power measurements

Figure 2.18 illustrates how the traceability chain is shortened with the developed fibre-coupled primary standard.

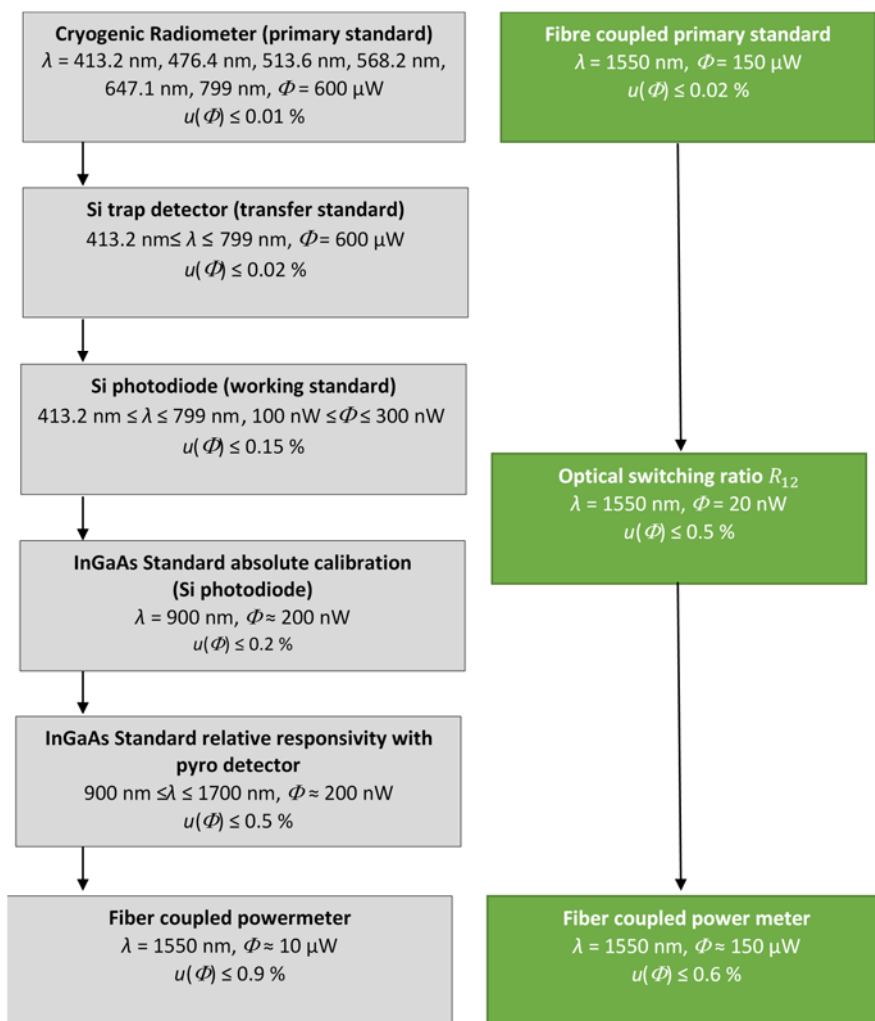


Figure 2.18. Traceability chains: On the left (Gray) the traditional traceability chain that uses as primary standard a free beam CR; on the right (Green) the shorter traceability chain that uses the fibre coupled bolometer as primary standard.

Results and conclusions

The attenuator was set to have an approximate optical power at the PCBC of about 155 μW . The reference setpoint temperature was set to have the PCBC TES at a working point of 3.98 K. Using the thermal link calibration data described above the software estimates the electrical high and low levels that surround the estimated optical power. The measurement itself consists of a sequence of 4 sets of series of optical-electrical low- optical – electrical high measurements for a total of 9 optical measured values. The standard deviation of the mean of the optical power measured is 150 ppm. During measurement of the electrical power the METAS optical switch is set to illuminate the CMI reference InGaAs detector.

Table 2.1. Results from comparison between bolometer and CMI InGaAs reference.

CMI InGaAs reference [μW]	CMI InGaAs reference repeatability %	Value measured by PCBC	SEOM % bolometer	Power at power meter (switching ratio)	difference DUT/bolometer %
173.22	0.12	154.57	0.016	172.28	-0.55

The novel absolute primary standard radiometer for optical fibre power measurement has started performing in CMI as a new primary standard detector providing one-step direct traceability of absolute optical radiation power measurements in optical fibres to the fundamental constants. The system solved the issues of current transfer standard detectors, i.e. spectral dependence and temporal drift, and shortened the traceability chain. This way it decreased the measurement uncertainty for more than 30 %, which moreover was achieved via a shorter and easier to maintain traceability chain. The achieved relative uncertainty was 0.3 %.

4.2.6 Summary of key research outputs and conclusions

Several calibration techniques and artefacts were developed, characterised and successfully validated to improve traceability of fibre-optic measurements.

Artefacts for the calibration of the distance scale of very high resolution Optical Low Coherence Reflectometers (OLCR) and of high-resolution photon counting Optical Time Domain Reflectometers (OTDR) were developed. These artefacts allow calibrating in a simple and accurate way, which was until now not available.

New artefacts for the calibration of the attenuation scale of multimode OTDR in an absolute way were developed, validated by comparisons and tested by interested industry partners. These artefacts offer a very simple method for accurate calibration of the absolute attenuation scale of multimode OTDRs. Promising discussions were started with the working group active in this field within the IEC, with the aim to evaluate the future improvement of existing calibration standards using these new calibration artefacts and techniques.

Two fully traceable instruments for the measurement of the Encircled Angular Flux (EAF) were developed and validated by inter-comparisons. The EAF allows quantifying the modal distribution in large core multimode step-index and in plastic optical fibres by evaluating the far-field intensity pattern. A careful control of the modal distribution is fundamental in order to ensure comparable and repeatable measurement of quantities like bandwidth and losses in multimode systems.

Different models were developed to calculate the modal distribution in multimode fibres and to simulate excitation of these modes by a focused beam, using finite-element methods (FEM). Software were successfully tested for the estimation of the coupling efficiency between two fibres. These results pave the way to the determination of Encircled Angular Flux templates using FEM simulations and thus to contribute to the development of the IEC normative documents in that field.

A novel absolute primary standard radiometer for optical fibre power measurement based on carbon nanotubes at cryogenic temperatures was developed. It acts now as a new primary standard detector providing in one-step direct traceability of optical radiation power measurements in optical fibres to the SI. The system solved the issues of current transfer standard detectors, i.e. spectral dependence and temporal drift and decreased the measurement uncertainty by more than 30 % and the achieved relative uncertainty was 0.3 %.

New calibration techniques and performance enhancement strategies for distributed and quasi-distributed fibre sensors were developed. A reference artefact for simultaneous resolution and temperature calibration of distributed fibre sensors was developed as well as two calibration methods for fibre Bragg grating interrogators, providing uncertainties down to ± 0.65 pm. All these methods have been incorporated to calibration capabilities already. Regarding sensor enhancement an OTDR with a photonic differentiation detector providing high resolution and sensitivity temperature measurements and a coherent-OTDR for distributed vibration measurement providing single pulse characterization with high resolution and sensitivity were developed.

4.3 Metrology of terahertz transmission links

This objective developed measurement standards and standard measurement procedures for terahertz transmission systems by investigating the operation, functionality and characterisation of devices used in THz links.

Metrology requirements and needs for THz communications were identified and metrology were discussed with collaborating partners, in particular industry partners, Toptica and Menlo, who are device manufacturers. This work aligns with the activities of a network of German THz manufacturers, which has been set up with the primary task of developing metrology standards for the industry, and a collaboration has ensued. Characterisation protocols for emitters and detectors used for THz transceivers and communication links were agreed with project partners. Measurement instruments were built for characterisation of THz components. A lamellar interferometer and a spatial beam profiler have been implemented and configured to characterise components employed in THz communication systems. Devices from both Toptica and Menlo were characterised. A THz transmission link was setup at NPL in collaboration with Toptica, and was used to demonstrate component characterisation.

4.3.1 Broadband spectroscopy at THz frequencies

A type of interferometer that is particularly suitable for broadband spectroscopy at THz frequencies is a Michelson interferometer with a lamellar mirror, shown in Figure 3.1, where a split mirror acts as both a beam-splitter and a moveable mirror. The lamellar mirror consists of two parts, each comprising several lamellae or “fingers”, with one part being fixed and the other moveable. This design avoids using a separate beam-splitting element; is polarization-insensitive; and can be ultra-broadband.

A lamellar interferometer can be used to determine the spectral performance of both emitters and detectors. To characterize an emitter, a calibrated power detector is required, having a flat response over the bandwidth of interest. The pyroelectric detector described above is suitable for this purpose, and will be employed. Of particular interest is the possible presence of features outside the fundamental emission line, such as harmonics and side-lobes, and their dependence on the bias voltage.

Conversely, to characterize a detector, a calibrated broadband source with a known spectrum is necessary, such as a black body. Several types of well-characterized sources are available and can be employed to measure spectral responsivity of receiver devices. The spectral NEP of a detector can be obtained if the noise spectrum of the source is known.

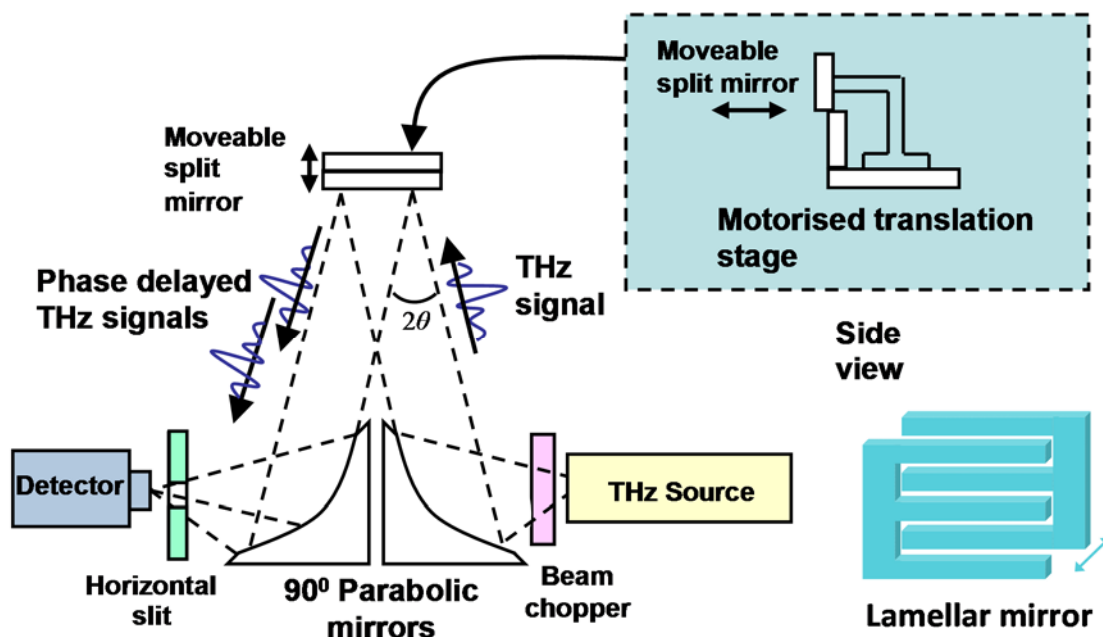


Figure 3.1. Schematic drawing of a lamellar interferometer and a split mirror.

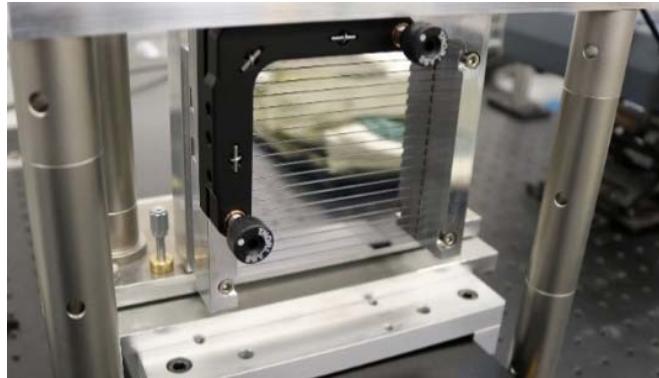


Figure 3.2. Photograph of the lamellar split mirror at NPL.

The operational bandwidth of the interferometer is determined by the number (N) and height (h) of the lamellae. The ratio of maximum to minimum frequency is roughly equal to the number of lamellae in each half of the mirror: $f_{\max}/f_{\min} \approx N$. The maximum wavelength is set by the lamellae height: $\lambda_{\max} < h/2$. The parabolic mirrors used for input/output must have diameter at least as large as the total height of the lamellar mirror. To maximize optical throughput, the width of the lamellar mirror should be equal to or larger than its height.

The instrument designed and built at NPL has a mirror with 20 lamellae in each half, each with a height of 2.5 mm (shown in Figure 3.2), making a mirror with a total height & width of 105 mm \times 105 mm. Its bandwidth at maximum sensitivity is therefore from 300 GHz to 6 THz. However, the shallow fall-off at lower frequencies allows measurements to be carried out down to <100 GHz.

The frequency resolution of a Michelson interferometer is determined by the scanning length of the moveable mirror, and is given by $\Delta f = c/2L$, where c is the speed of light in air and L is the scanning length (with the factor 2 arising due to double-pass). Typical achievable resolutions are of the order of 1 GHz, which is much coarser than that of a signal analyser. Unlike electronic spectrum analysers, a free-space lamellar interferometer is not a commercial instrument. Attention therefore must be given to its testing and calibration. The bandwidth, however, is very large: with a suitable detector, a bandwidth of a decade or more is easily obtainable. Moreover, because these devices operate in free-space, the bandwidth is not limited by waveguide transmission.

The dynamic range of spectral measurements using the lamellar interferometer depends on the emitter noise and the dynamic range of the detector employed.

Emitter spectral profile measurements

Figure 3.3 presents examples of source spectra obtained with the lamellar interferometer. Figures 3.3a and 3.3b demonstrate the effect of harmonics, and that the presence of a harmonic component can be clearly detected (this is not possible using a narrow-band frequency analyser).

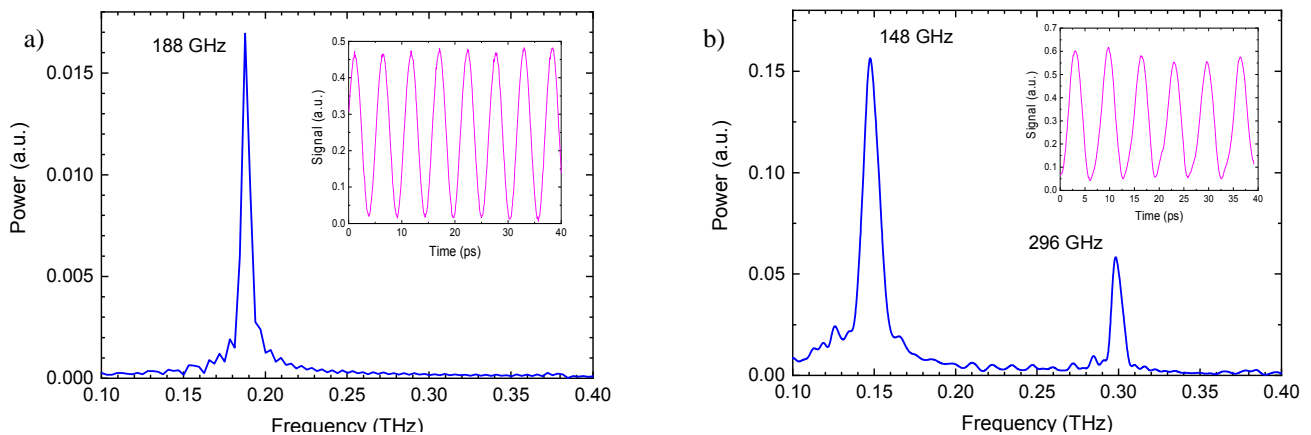


Figure 3.3. THz source spectra obtained by a lamellar spectrometer. Insets show detector signal. a) Source at a nominal 190 GHz, no harmonics. b) Source at a nominal 150 GHz, strong 2nd harmonic present.

The dynamic range of these measurements in frequency domain was approximately 100 (10 dB). The frequency uncertainty in the peak position was determined by the data point spacing, and was ± 1 GHz. The uncertainty in peak maximum was 5 %.

4.3.2 THz beam imaging

The simplest technique for observing the beam profile of an emitter is to employ a detector with a small aperture, which is raster scanned across the beam area while recording the received power (Figure 3.4). This is repeated at different distances from the emitter to derive beam divergence. Alternatively, the detector may remain stationary, with the whole of the beam being collected and focused onto it (by mirrors or lenses), while only the aperture is scanned across the beam. In this case care must be exercised to avoid errors due to edge diffraction at the aperture. The spatial resolution is limited by the emitter power and detector sensitivity. This method will be the first-step approach adopted for emitter beam profile characterization. Good accuracy is easily achieved using this technique, and its implementation is straightforward, but it is slow and cumbersome. Since only power is measured, it also suffers from inability to provide phase information.

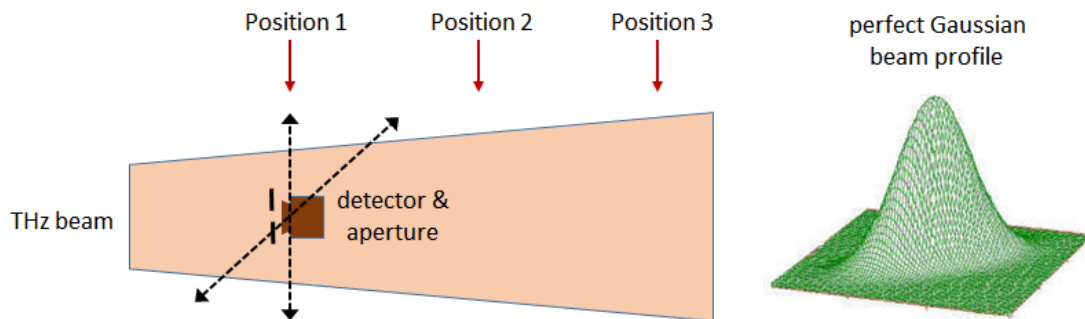


Figure 3.4. Schematic drawing of beam imaging by aperture scanning.

THz detector acceptance cone

The acceptance cone of a detector is the dependence of its responsivity on the beam incidence angle. It can be determined using a goniometer-like arrangement, shown in Figure 3.5. The detector is rotated along both axes orthogonal to a well-collimated beam, and the signal dependence on the angle between the beam and detector axes denotes the acceptance cone.



Figure 3.5. Schematic drawing of measurement of acceptance cone of a detector.

Emitter beam profile measurements

Industrial partners expressed particular interest in measurements of beam profiles of their emitters. We therefore focused our attention on this area, employing the scheme depicted in Figure 3.6.

Figure 3.6 presents examples of measured beam profiles from Emitter 1, at a distance of 10 mm, together with Gaussian fits. This emitter is a continuous-wave photoconductive mixer with a tuneable frequency. It is seen that its beam profiles are approximately Gaussian, but with additional weak features. Whereas the width of the beam remains constant with frequency, the features vary.

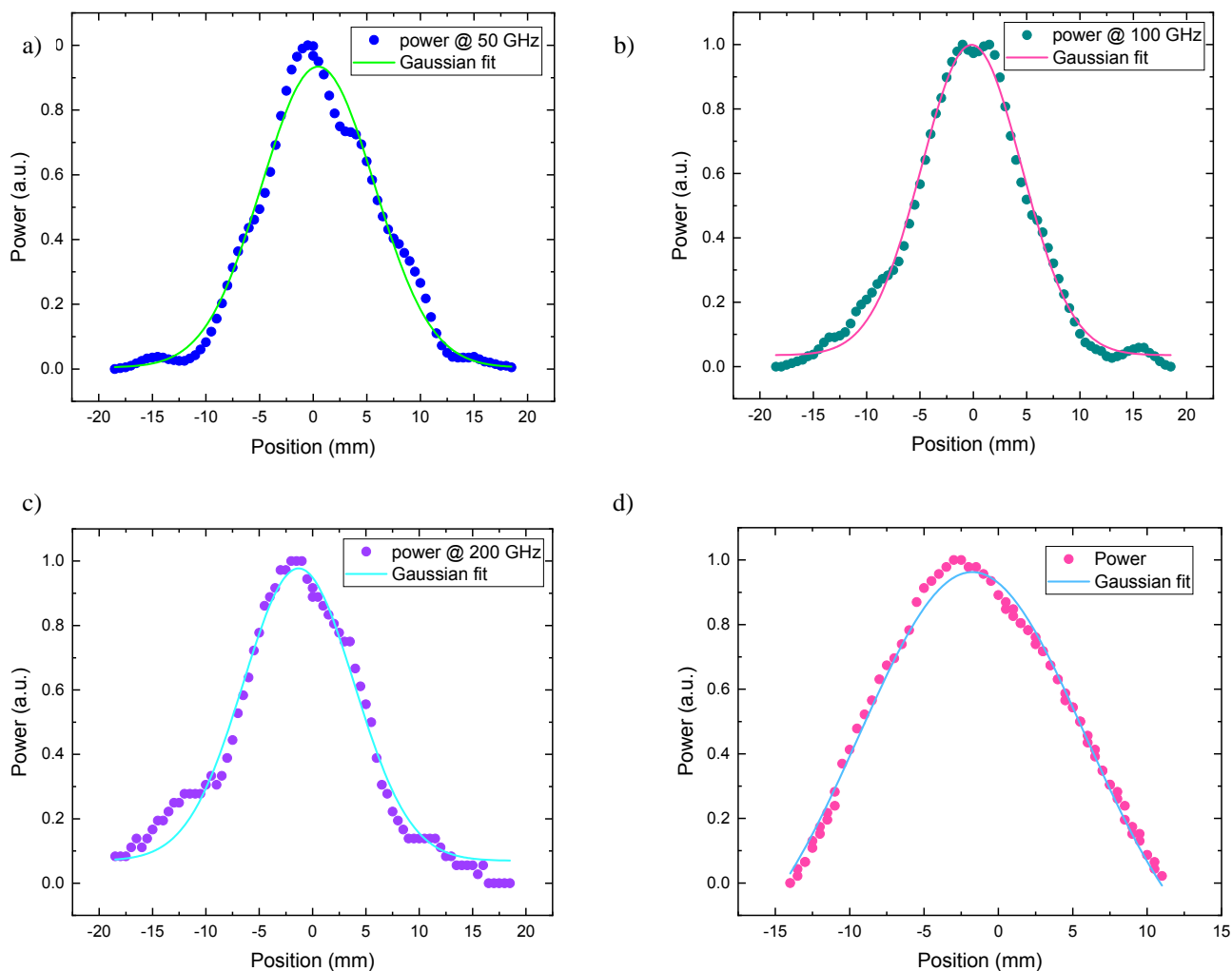


Figure 3.6. Examples of measured beam profiles from Emitter 1 at distance of 10 mm: a) at 50 GHz; b) at 100 GHz; c) at 200 GHz. d) Example of measured beam profile from the Emitter 2 at distance of 10 mm, together with a Gaussian fit. This emitter is a pulsed photoconductive source with broad bandwidth of 0.1–4 THz. The power detector measures average integrated power. It is seen that its beam profile is approximately Gaussian. The beam width is about 50 % larger than that of Emitter 1, and it lacks features.

The dynamic range of the beam profile measurements was approximately 100 (10 dB). The amplitude uncertainty was approximately 15 %. However, since this was random error on each data point, the resulting uncertainty in the beam profile was only around 5 %. The position uncertainty was ± 0.1 mm.

Detailed reports of the beam profile measurement results were prepared and sent to the industrial partners.

4.3.3 Insertion loss measurements

A THz transmission link was set up at NPL using Toptica emitter and receiver, and was used for characterisation of passive components. Characterisation measurements include insertion loss of filters, beam-splitters and windows, and beam-forming properties of lenses.

Figure 3.7 shows an example of insertion loss measurement of a waveguide filter made by Protemics (Protemics GmbH, Germany). The dynamic range of the filter is 12.5 ± 0.5 dB (4 % uncertainty). The mean uncertainty in the loss measurement (shown by error bars) was 3 % (well within the target of <5%).

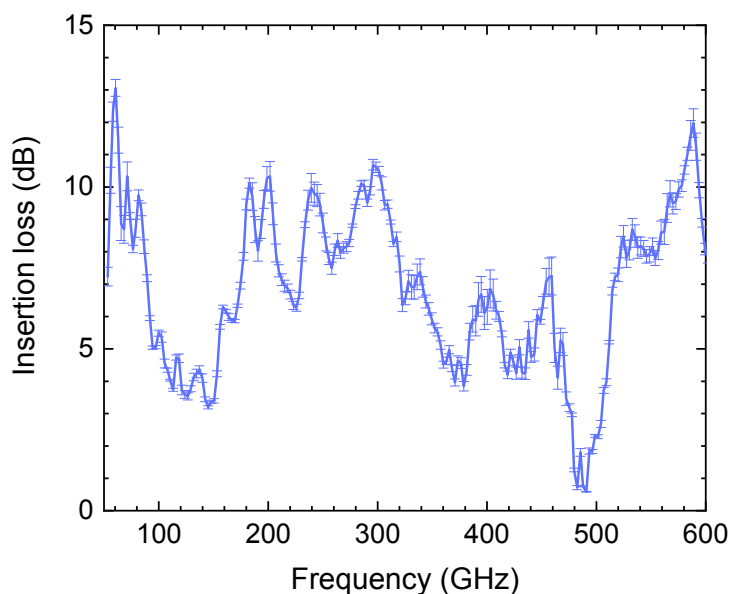


Figure 3.7. Example of measured insertion loss of a Protemics filter. The dynamic range is 12.5 ± 0.5 dB; the mean uncertainty in loss measurement is 3 %.

4.3.3 Summary of key research outputs and conclusions

The project developed measurement standards and standard measurement procedures for THz transmission systems by investigating the operation, functionality and characterisation of devices used in THz links.

Characterisation of THz emitters and detectors require measurement of a number of different parameters but at present only the power and frequency of emitters can be measured to adequate metrological standards. The project developed methods for reliable determination of spectral performance and emitter beam profiles, as these were identified by industry partners to be the most important parameters that could not be measured.

A lamellar interferometer suitable for broadband spectroscopy at THz frequencies was designed and built. It was used for emitter spectral profile measurements of devices from industrial partners. The uncertainty for dynamic range in these measurements was found to be better than 5 %. A spatial beam profiler was implemented and configured to characterise emitter beam profiles and detector acceptance cones. Beam profiles of emitters provided by project industrial partners were measured successfully. Moreover, a THz transmission link was set up and used for characterisation of passive components, e.g. insertion loss of filters, beam-splitters and windows, and beam-forming properties of lenses. The mean uncertainty in the loss measurement was 3 %.

4.4 Establish metrology tools for performance characterisation of polymer waveguides mounted on electronic circuit backplanes used in high-speed data links

The aim of this objective was to develop suitable measurement systems that can characterise the functional performance of waveguides incorporated onto short range interconnect boards. Therefore, metrology was developed for optical printed circuit boards (OPCB) by implementing a characterised measurement system incorporating a variable launch condition to monitor board performance under a range of controlled environmental conditions. Moreover, three coupling approaches were investigated to physically implement fibre-to-chip access to integrated optical circuits.

4.4.1 Characterisation of optical waveguides under different environmental conditions

The continuing high growth in the world's data traffic has led to many improvements in both fibre and detector technologies. Along with these developments has been the need to develop short range optical links within data centres to reduce the bandwidth bottleneck providing seamless connectivity from external optical

networks. Optical links on a pluggable daughter board offer vastly improved data transfer speeds compared with copper (typically >40 Gbps compared to <4 Gbps for copper). These links are embedded onto PCB boards and are known as electro-optical optical circuit board (EOCB's). Broadly, these boards fall within three technologies: Fibre-optic laminate, polymer waveguides and planar glass waveguides.

As the technology rapidly develops, there is a corresponding need to provide characterisation of these boards for the key operational parameters such as attenuation, isolation (crosstalk) and bit error ratio (BER) as well as a need to provide standardisation through the activities of international standards bodies.

The principal partners involved with the characterisation of the EOCB's waveguides were Seagate and Arden Photonics. Meetings with Richard Pitwon and Kai Wang at Seagate provided industry advice on the state of the art regarding this technology as well as guidance on the proposed measurement strategy. In addition, relevant standards developed by Richard Pitwon under Working Group TC86 (IEC 62496-2:2017 (E)), provided crucial up to date guidance for setting up and specifying the launch condition as part of the measurements. Seagate supplied the reference EOCB required for the measurements carried out at NPL. The board incorporates waveguides 70 μm by 30 μm in cross section and consists of 11 waveguide groups of structures that include planar, splitters and radii. The waveguides are Siloxane based polymers. This board was previously assessed under the previous Phox Trot European Research Project (<http://www.phoxtrot.eu/>). Arden Photonics provided advice on the use of the Modal Explorer and interpretation of data when assessing the energy distribution and modal conditions of the launch and received signals. NPL, Seagate and Arden Photonics are members of BSI committee GEL86 – Fibre Optics, GEL/86/2 – Passive components and interconnecting devices and GEL/86/3 – Fibre optic systems and active devices.

Total Attenuation Across Thermal Range

The Seagate board was mounted on a large X,Y,Z translation stage. It was secured using silicone gel pads that provided a method to prevent the board from moving during the measurement runs and to counter any possible low frequency vibrations. Careful alignment was necessary to ensure that the launch spot was centrally located onto the front facet of the selected waveguide. A suitable neutral density filter was used to ensure that the reference measurement did not saturate the camera. The receive board was brought into place and alignments carried out to ensure the image of the illuminated waveguide was centrally placed on the CCD.

The signal image was analysed to find the centre of the intensity and the total power was found by summing all the pixels contained within a circular area around this centre. The diameter of this virtual pinhole was adjusted to capture all the light exiting these waveguides. In the case of these relatively large waveguides a 150 μm virtual pinhole was used. To calculate the attenuation, the total input divided by the reference for the input image was divided by the total output divided by its reference. This measurement technique provides the insertion loss of the waveguide under test, which includes the waveguide loss and the input and output coupling losses. Results for the selected waveguide are shown below. Clearly, the increase in applied thermal load indicates a small but observable increase in the total attenuation. The maximum range of the measured total attenuation (includes coupling losses) is ~ 0.3 dB using the 90 x 30 mm shroud centrally placed over waveguide group. The expanded uncertainties associated with the measurements are estimated as ranging from U95 < ± 0.1 dB @ 20°C and ± 0.20 dB @ 80°C.

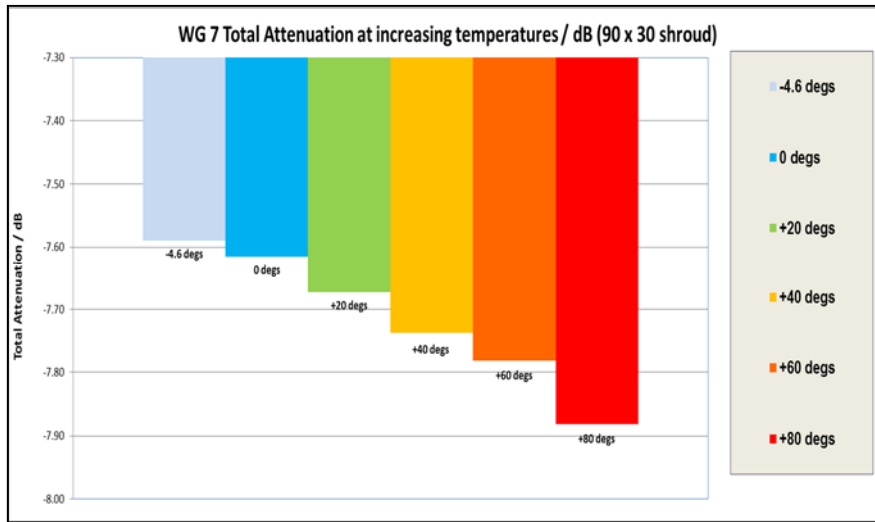


Figure 4.1. Total attenuation results for waveguide 7 across different applied hotspot temperatures.

Encircled Flux Across Thermal Range

The board was setup and the output facet of the waveguide was placed against the Arden Photonics MPX-1 Modal Explorer. Care was needed to optimize the focus of the output spot onto the detector of the Modal Explorer prior to measuring the EF. Initial alignment was helped by using a HeNe laser fed into the launch setup before reconnecting the 850 nm VCSEL source. Once optimized, EF measurements were made covering the same thermal range as for the attenuation measurements and the same size of shroud and position on the board. Measurements were carried out on waveguides 5 and 7 using 1000 averages in order to capture the modal energy distribution. In each case the ambient temperature was recorded.

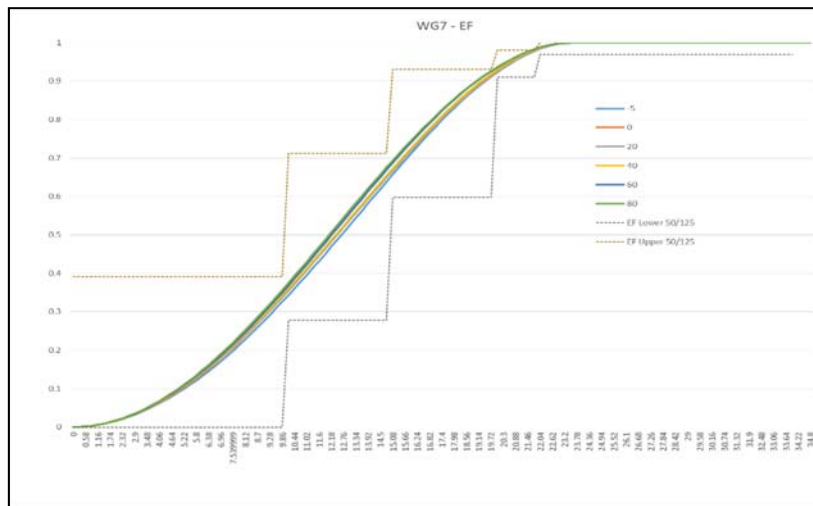


Figure 4.2. Encircled Flux results for waveguide 7 across different applied hotspot temperatures.

As with the total attenuation, the increase in applied thermal load indicates a small but observable shift in the Encircled Flux profiles consistent with higher order modes being decoupled from the guide due to the effects of the increased thermal load upon the guide and associated changes in the core cladding refractive index ratio. This progressive shift is significant as it approaches and exceeds the limits defined by the EF templates as specified in IEC 61280-4-1/Ed3/CD:2015 especially at the elevated temperature of 80°C. If this is the case then subsequent measurements would fail the specified criteria required by the IEC standard. Preliminary uncertainties estimated for the EF measurements at the worst case repeatability of 80°C give a U95 of +/- 0.0045.

Bit Error Ratio (BER) Measurements

Bit error ratio (BER) measurements were performed on the optical waveguide to assess potential degradation in performance over the two extreme temperature range $-4.4\text{ }^{\circ}\text{C}$ to $80\text{ }^{\circ}\text{C}$.

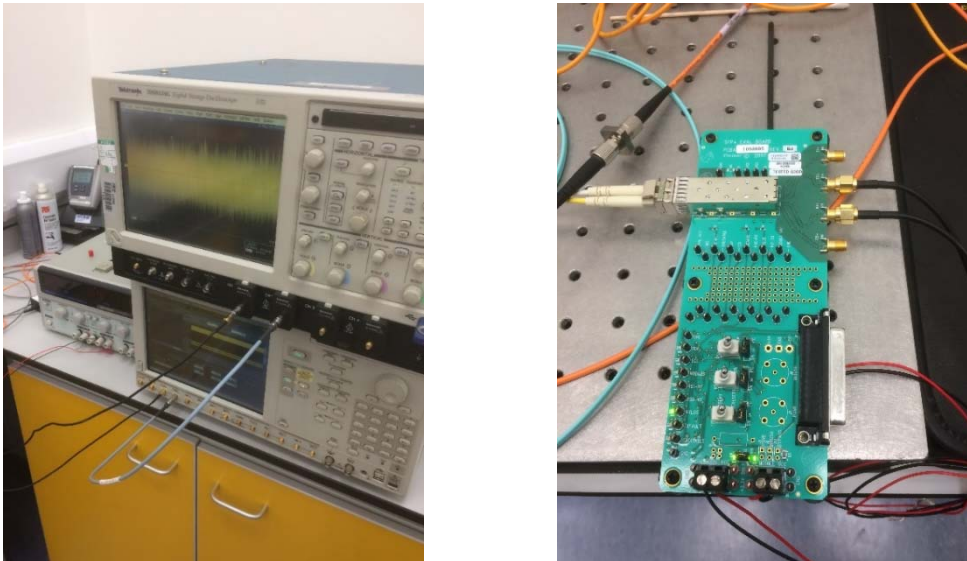


Figure 4.3. Experimental setup to generate and detect the electrical signals from the arbitrary waveform generator. The SFP+ transceiver module is also shown.

Experimental setup to generate and detect the electrical signals from the arbitrary waveform generator. The SFP+ transceiver module is also shown.

An arbitrary waveform generator was used to generate a pseudo-random binary sequences (PRBS) electrical signal to drive an SFP+ transceiver module. The intensity modulated signal was launched on channel 2 and 7 of the waveguide (WG2 and WG7) through a modal conditioner. The transmitted signal recovered from the photo-receiver was analysed on a real-time oscilloscope sampling at 20 GSa/s.

The BER was measured at the two extreme operating temperatures ($-4.4\text{ }^{\circ}\text{C}$ to $80\text{ }^{\circ}\text{C}$) using the Thermostream chamber. The BER results are shown below. As can be seen, some degradation was observed for the transmitted data for the extreme temperature range $-4.4\text{ }^{\circ}\text{C}$ to $80\text{ }^{\circ}\text{C}$ for both waveguides WG5 and WG7.

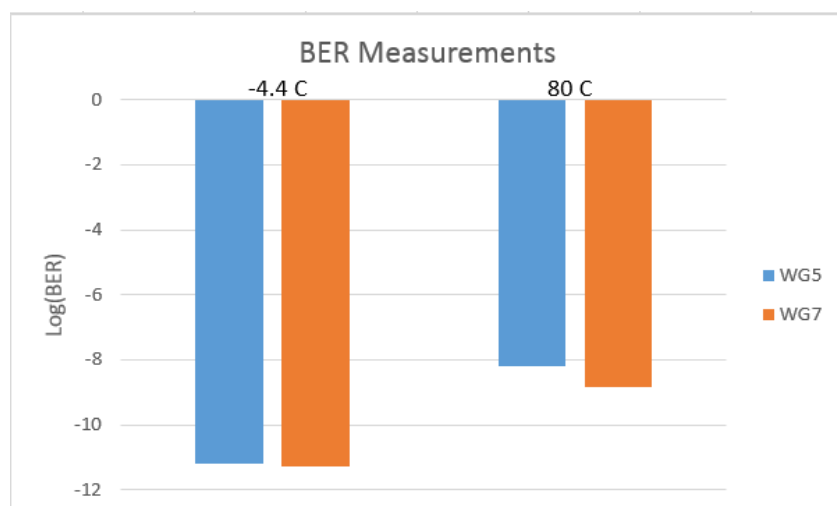


Figure 4.4. BER measurements on WG5 and WG7 of the OPCB for the two extreme operating temperatures ($-4.4\text{ }^{\circ}\text{C}$ to $80\text{ }^{\circ}\text{C}$)

The degradation in performance can be attributed to the increased total attenuation over the temperature range.

Conclusions

The work undertaken has been an important step in understanding the functional performance of these emerging polymer waveguides within application environments where the guides themselves are expected to be in very close proximity to other thermally generating components. The hybridisation of these boards in which optical and copper based tracks lay in close proximity with these other components. Testing of a board's and polymer waveguide's integrity has been carried out in the past with the subsequent performance being assessed in terms of attenuation and BER. Up till now, the actual characterisation itself has largely concentrated on the performance of these waveguides under ambient lab conditions.

For the various measurement parameters, observable changes were measured that correlated with the applied thermal load. By applying the same controlled launch conditioning to three different parameters, observable changes were measured that correlated with the applied thermal load. Significantly, increases in thermal load to a controlled section of the waveguides under test show decreases in total attenuation and associated drop in the BER. The Encircled Flux measurements reveal a corresponding shift in the power distribution across the waveguides resulting in a compromising of the prescribed standardised EF limits. These thermal loads, emulating associated component hot spots, directly affect the nature of the polymer and cladding and their refractive index relationship. The applied thermal load indicates a reduction in the refractive index differential ($\Delta n/\Delta t$), allowing subsequent leakage of the propagated light into the surrounding cladding. This is seen through the shift in the EF profile and explains the noticeable loss in total attenuation and corresponding reduction in BER as the temperatures applied to the waveguides is increased.

This research has far reaching consequences for board designers, manufacturers and standards bodies. The unavoidable increase in board complexity and hybridization, in the drive to accommodate higher and higher data rates, will need to take into account these performance and functional limitations imposed by the application of thermal loading.

4.4.2 Fibre-to-fibre coupling in high power applications

The aim of this task was to evaluate the applicability of common characterisation methods for fibre interconnects to high power operation.

Oplatek brought insight on what kind of experiments are important for industry as well as fabricated and provided special connectors for testing. FhG designed and implemented a measurement setup allowing characterization of fibre connectors at up to 10 W of laser power. This is sufficient to hit the power range at the damage threshold of standard connectors. A first set of connectorized test fibres was selected, acquired and characterized, yielding power dependence of the connector loss. It was observed that high quality connectors (AVIM, Mini-AVIM) keep up their performance as specified at lower power when used at Watt-level average power. In contrast, standard connectors (FC/APC) exhibited increased loss when operated at more than 300 mW. The error of the measurements could be kept below 5 % (with respect to the power meter) for higher powers, mainly caused by power fluctuations of the test laser and the thermal power meter head. Thermal observations (by thermal camera) were also performed, but did not yield significant results. On the one hand, most connectors only had metal housings, which makes observation of temperature by camera nearly impossible, on the other hand, the heating was just not significant enough.

Spliced connections of high power fibres were analysed using refractive index tomography. In particular, splices with a constant product of splicing arc duration and arc power were investigated for the critical connection between large-mode-area Tm-doped fibres and their matched passive counterparts. To evaluate the impact in high power fibre amplifier systems, beam propagation simulations were performed using the measured refractive index profiles, with different longitudinal resolutions of the tomography being applied depending on the observed refractive index changes due to dopant diffusion. The original plan was to use FEM simulations by JCM software but it was found out that the calculations could be done by a much simpler method. The transverse heat profile was calculated from the measured core temperatures of a high power thulium fibre amplifier. Using these measured core temperatures, the influence of the thermally induced transverse heat profile and the corresponding thermos-optical changes in refractive index on the mode profile was calculated. From these mode profiles, the change in splice transmission and in higher order mode excitation caused in by thermal effects in high power operation could be deduced by mode field overlap calculation. It should be noted that the case of a thulium system, causing temperature increases of 80 °C and more at ~100 W due to large quantum defect, is a worst case for such a splice. In ytterbium-based systems, common temperature increases are in the range of 10 °C for kW average power. Nonetheless, it was found that the increase in temperature did not cause significant changes to splice quality. Previously bad splices (too hot / too long) even exhibited slightly increased transmission, whereas good splices did not deteriorate.

A test set of 20 cladding light strippers based on high index UV-curing adhesive was produced. Five different well-defined bending radii of the employed no-core fibre were considered, with 4 different lengths of adhesive each. For characterization, the transmission in dependence of the parameters was measured both spectrally and regarding the numerical aperture (NA) of the output light. While the spectral transmission, using a white light supercontinuum source, showed no distinctive features, the transmission was seen to depend highly on the NA of the guided light. Lower numerical apertures are only slightly attenuated, e.g. between 5.5 dB and 11 dB for light with NA below 0.1, depending on the cladding light stripper (CLS) length, for a straight fibre. This value can be significantly increased by bending the fibre in the device, going up to about 20 dB for bending radius of 7 cm at 4 cm CLS length. This allows to greatly increase the efficiency of such a component, which is crucial for high power fibre systems. Due to the destructive nature of reference measurement, and because the input coupling plays a role in modal excitation and thus the angular distribution of the light in the CLS, no direct measurement of repeatability could be performed. However, the standard deviation of the measured angles to certain power levels was usually between 1% (reference measurement) and 4% (CLS measurement), limited by the goniometric instrument due to the required electric amplification. This yields a (very) rough estimate of 5% for the total standard deviation of the angular transmission.

4.4.3 Demonstration of a mirror enhanced low-loss grating coupler, a 3D broadband coupling device and 3D printed coupler

Fibre to chip coupling is essential to connect micro- and nanostructured optical components to macroscopic dimensions and to the telecommunication infrastructure. For this purpose, efficient and functional interfaces between planar on-chip optical components and out-of-plane fibre device have to be established. In particular, for devices with multiple optical access ports several coupling interfaces are required for convenient and reproducible device readout.

In order to physically implement fibre-to-chip access to integrated optical circuits, three coupling approaches were investigated theoretically by numerical studies and through experimental implementations. These approaches include both planar on-chip devices as well as three-dimensional components realized with DLW and micromolding. Realistic device parameters were extracted from numerical simulations and fed into the later fabrication process chain. Experimental realizations for mirror enhanced grating couplers and 3D couplers fabricated by direct laser writing were demonstrated within the project.

Following the design and simulation several rounds of devices were implemented in hardware for grating structures and also for 3D DLW couplers. These results fulfil the requirements on low-loss coupling for the grating devices as specified in the proposal, as well as broad optical bandwidth for the DLW written devices. 3D printed couplers were investigated by simulations only. Below a more detailed description of the work.

The coupler design and experimental realization was carried out in close collaboration with all project partners. Details on the implementation and final configuration were discussed in depth at the project meetings and during conference visits. Design parameters and geometries were further shared between project partners during the project work, in particular with respect to numerical verification of experimental designs. This way the coupler parameters were devised according to the project goals and were adjusted to the needs of the individual project partners. This in particular concerns the collaboration with METAS for the design of chip-scale artifacts, which rely on efficient grating coupling for optical readout.

The final coupler designs relied on the close interaction between the fabrication partner WWU and the design partners from industry and academia. Numerical simulations were employed to optimize the experimental designs. These were carried out in close collaboration with JCM and UEF and concerned all types of couplers explored within the project.

Experimental results were obtained in close collaboration with NPL, FHG and CSIC. Only through this interplay between experimental measurement and simulations, the final designs were accomplished. Thus, the collaboration within the project was crucial to arriving at the high coupler performance in the end. Industrial exploitation was targeted together with Seagate, while further scientific dissemination was achieved with METAS.

Realization of mirror enhanced grating couplers, numerical simulations and results

Grating coupling devices employ Bragg refraction to couple out-of-plane light into in-plane propagating optical modes on a chip. Using low diffraction orders allows for emitting light under an angle from a waveguide, as well as coupling external light under an angle into a waveguide. The optimal coupling efficiency is obtained, when the Bragg diffraction condition is obeyed, which is why the coupling bandwidth is typically centred around a given wavelength determined by the geometry of the grating, especially the grating period. Changing the

filling factor of the grating on the other hand affects the coupling efficiency and also the coupling wavelength to a weaker degree. Simple gratings are transferred by top down nanofabrication into the waveguiding material using etching methods. Without adaptation, parts of the incoming light fields is lost into the substrate. Therefore, the grating structure has to be adapted to collect all light contributions for waveguide coupling. In order to do so, in this subproject metallic mirrors were employed to backreflect light transmitted into the substrate into the grating to increase the overall coupling efficiency. Because of interference between the incoming light beam and the reflected light beam suitable designs of the layer stack had to be performed. Inherent to grating structures is a limited bandwidth around the central coupling wavelength.

The mirror enhanced grating couplers were numerically designed to obtain maximum out-coupling efficiency and fulfil mode-matching with a gaussian-like mode. Waveguide tapering length and grating coupler size were optimised. In particular, shortening the tapered section down to few μm requires the introduction of bent grooves to match the rapidly expanding phase front from the guided mode with the one (almost flat) of the free-space gaussian mode. The optimization of the coupler was then based on 2D finite element simulations performed using COMSOL MULTIPHYSICS commercial software. A 2D representation for the couplers is indeed effective since, after tapering, the waveguide is more than $3\ \mu\text{m}$ wide, and the effects of the lateral confinement with respect to the bulk medium are negligible (change in the effective refractive index $< 5\ \text{‰}$).

In order to further simplify the computational problem, we focused on the optimization of the output coupling from the guided mode to free space. Fig. 1a is a sketch of the simulation setup: a line source (1) is placed inside the Si_3N_4 waveguide (2), which is set long enough to select the guided part of the radiation; artificial absorbers are also placed to dump uncoupled light (3). The coupler structure is then composed by a gold layer (4) that covers the HSQ cladding (5) of the fully etched grating. Regions (6) and (7) correspond to air and glass substrate, respectively. The coupling efficiency is calculated as the ratio between the power flow through the output detector (8) and the reference detector (9). The detector (8) is also used to evaluate the transverse profile of the output beam in free space (Fig. 1c). The domain of simulation is terminated with perfect matching layers (PML)(10), to avoid un-physical reflections. The output of the optimization procedure is a grating coupler composed of 18 grooves, with the 9 closer to the guide following an apodization recipe and the others keeping a constant filling factor (Si_3N_4 portion of a period) between 50 % and 65 %.

Input and output coupling are optimized around 785 nm under an angle of about 8 degrees through the glass substrate. This angle is enough to suppress reflections into the waveguide due to second order Bragg scattering, while keeping the beam within the numerical aperture of the objective. The HSQ cladding reduces the scattering strength of the single grating element, serves as a buffer layer to set the mirror at the optimal distance for constructive interference toward the glass, and prevents the formation of anthracene crystals in the coupler areas. The maximal coupling obtained in simulations reaches 90 %. In order to obtain more robust performances however, the parameters of the fabricated structures slightly deviate from the ideal ones, and considering also the effect of the 10-nm adhesion layer of chromium, the expected coupling efficiency is reduced to around 60 %. Finally, in order to match the free space output mode with the laser quasi-Gaussian profile, we first act on the apodization recipe to improve the symmetry of the longitudinal profile (see Figure 4.5), and then choose a waveguide tapering length of $4.5\ \mu\text{m}$ so as to set the transverse size similar to the longitudinal one.

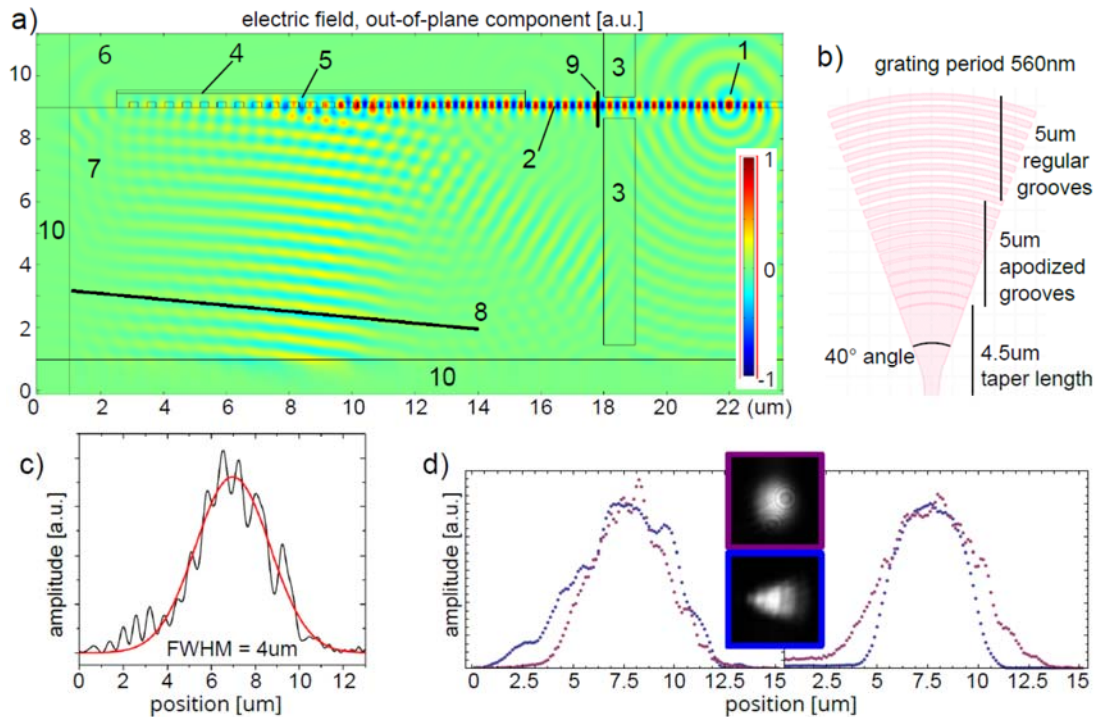


Figure 4.5: Grating coupler simulations. a) Out-of-plane component of the electric field distribution in the case of 89 % coupling efficiency. The guided mode is pumped by a line source (1), and the amount of light directed toward the output direction after scattering on the grating region (5) is evaluated as the energy flux through the detector line (8). b) Geometry of the couplers. Parameters used for fabrication: HSQ layer thickness 750 nm; grooves width 280 nm (regular series) and 50-50-65-80-95-120-150-180-180 nm (apodized series). c) Simulated intensity profile of the output beam (flux through the output detector (8)) for the fabricated gratings (black solid line) and Gaussian fit to it (red solid line). d) Intensity profile along the direction of the guide (left) and orthogonal to it (right), measured for the coupler output (blue dots) and for the retro-reflection of the laser spot (purple dots).

After numerical optimization, mirror enhanced grating coupling devices were realized by nanofabrication in several lithography steps combined with reactive ion etching and lift-off processing. Nanophotonic devices are prepared from 175 nm stoichiometric Si_3N_4 on top of 500 μm glass substrates. The fabrication was performed by three steps of electron-beam lithography followed by reactive ion etching. This way many coupling devices can be realized in a single fabrication run and be experimentally measured using fibre optical equipment.

Mirror-enhanced grating couplers were fabricated as outlined above and characterized via transmission measurements. These measurements consist in spectral characterization of the on-chip devices by sending light from a tunable laser source into the chip and recording the transmitted optical power in dependence of wavelength. This way the coupling bandwidth and spatial coupling characteristics can be assessed for each fabricated chip design.

In Fig. 1d we show the coupler mode as imaged in transmission measurements. The agreement with simulations is remarkable, as it is evident by comparing the spot profile with the reflection of the laser beam on a silver mirror (line-cuts from EMCCD images, blue and purple dotted line, respectively). Indeed, the numerical evaluation of the overlap integral between the two spots yields values higher than 0.9. From transmission measurements, we obtain optical coupling bandwidth of roughly 30 nm in the near-infrared wavelength regime. Best transmission values at the central coupling wavelength show transmission of over 70 % well within the specified transmission window outlined in the proposal. We further find that the central coupling wavelength can be varied freely over a wide wavelength range, from visible wavelengths at 532 nm all the way to telecommunication wavelengths in the C-band around 1550 nm.

Being fabricated by top down lithography, the devices provide a scalable architecture. Beyond two-terminal devices, we have realized photonic circuits with up to 16 input ports each equipped with a grating coupling devices. These circuits can be read out in parallel using fibre arrays with a fixed fibre core distance matching the on-chip separation between individual grating coupling devices.

Realization of 3D couplers, numerical simulations and results

In order to overcome optical bandwidth limitations inherent to grating designs, we investigated tapered coupling structures that adapt the mode diameter of an optical fibre to a waveguide by creating an adiabatic transition between the two dimensions. Since fibres are aligned out-of-plane to the chip, this required access to three-dimensional structures, which also transform an angled fibre to a planar waveguide. Such architectures are feasible by using three-dimensional direct laser writing (DLW) into polymer photoresists for advanced nanofabrication. Crucial for the combination of planar devices with three-dimensional nanostructures are suitable alignment procedures by which free-form structures can be attached precisely at desired locations on prefabricated chips. Such alignment can be achieved by marker search and image processing. This way planar precision lithography can be conveniently combined with additive manufacturing techniques such as DLW.

Besides bandwidth limited grating coupling structures adiabatically tapered three-dimensional devices were investigated. For the design of such coupling devices, JCM developed interfaces that allow efficient computing and optimizing optical properties of grating couplers. The scripts were tested and updated for giving access to newly developed numerical methods, which were implemented in the finite-element method solver JCMsuite. Both the interfaces as well as the solver were made available to project partners within the consortium.

The newly developed methods include so-called *hp*-finite elements. These rely on the fact that best convergence properties for typical application cases are reached when an adaptive refinement of several interdependent numerical parameters is used. Adiabatic tapered devices, which extend beyond the chip surface, were simulated using this software for later implementation at WWU. The coupling architectures were simulated in a 2C cross-section as in the case grating couplers. Through the simulations, the modal distribution within the coupling device can be assessed and adapted to later experimental realizations. Performance was also demonstrated for tapered waveguide couplers with complex 3D geometry.

Experimentally such numerically optimized couplers were implemented by attaching 3D free form structures to previously fabricated planer waveguide circuits. These devices consisted of tapered waveguides onto which ends the 3D couplers were fabricated using DLW. The waveguide ends were determined using marker search and alignment to alignment structures realized during electron beam lithography. This way also many coupling ports could be realized in a single fabrication run. Typical writing times for 3D couplers involve 10 minutes of DLW using galvo scanning. Further optimization is possible through adjustment of the printing resolution as well as the scan path, in combination with speed enhancement of the writing tool.

In order to obtain wider coupling bandwidth, the 3D devices simulated by JCM wave were fabricated at WWU using a combination of planar lithography (EBL) and 3D DLW. With EBL photonic circuits with waveguides terminated by angled ends were realized. These waveguides expand the optical mode into free space if no additional photonic component is realized on chip. At the same time, alignment markers were realized alongside the waveguides for performing DLW after fabricating the waveguides. These alignment structures enable automatic marker search by the lithography tool such that multiple waveguides can be equipped with 3D couplers in a single fabrication process.

Following reactive ion etching of the waveguides, 3D couplers in the form of adiabatically tapered horns were attached to the tapered waveguide ends. The horn structures expand the waveguide mode towards the mode field diameter of an optical fibre. In the telecommunication regime, this amounts to horn diameters beyond 10 μm and thus still compact devices. In order to achieve collimated beam profiles the tapered couplers are equipped with optical lenses realized in the same fabrication run. Reflective coatings have not been applied to the top surface for ease of fabrication.

Different couplers geometries were investigated in order to optimize insertion loss and coupling bandwidth. Varied parameters include the coupler length, the outcoupling angle, the lens curvature as well as the top diameter of the tapered end. Multiple coupling devices were realized on each EBL fabricated chip using marker search and alignment. This way several coupling parameters could be assessed on each chip.

The device performance was measured via transmission characterization with a tuneable laser source for the telecommunication band and a white-light source for broad transmission characterization in combination with an optical spectrum analyser. Measured results for best devices reveal minimum insertion loss of -1.4 dB at a coupling bandwidth from visible wavelengths to telecommunication wavelengths. In the visible wavelength range, waveguide devices optimized for 1550 nm transmission show multi-mode behaviour, yet allow for efficient incoupling of light into the waveguide modes. The coupling structure did not show degradation over time and remained mechanically stable even after contact with fibre arrays. Through marker search and alignment, the fabrication approach is scalable as well to enable photonic circuit devices with multiple input ports. Structures circuits with up to 16 individual horn couples were realized and measured.

Realization of 3D printed couplers, numerical simulations and results

In addition to the free-form structures and grating devices, in a third design a combination of both approaches is used to realize coupling devices for higher power applications. In this case, an optical fibre is placed in direct contact with a nanofabricated chip lying flat on the chip surface. The end facet of the fibre is terminated with a prism structure realized by micromolding. The prism redirects light propagating through the fibre towards the chip surface and thus converts in-plane light to an out-of-plane beam. For better reflectivity, the prism surface is covered with a multilayer reflective coating. On top of a waveguiding thin film a grating structure is realized also by micromolding. Onto the grating the fibre and prism structure are attached, such that the reflected light beam from the fibre is coupled into the grating and subsequently into the waveguiding layer.

In our third design, 3D printed couplers as illustrated in Figure 2 were designed for later fabrication in the project. In this design, light from the optical fibre is connected to the substrate thus allowing light coupling to the chip for information processing or related techniques. Being a reciprocal device, the same approach allows for coupling light from the chip back into the fibre. Through a pair of such coupling devices a full transmission measurement circle can be established.

The coupling architecture comprises of a molded grating, combined with a reflective multilayer processed at an angle on the optical fibre with the help of a printed prism. The prism-structure is 3D printed to form an angled structure that connects the fibre to the substrate where the grating pattern is molded. The 3D printed structure is used cover the molded grating.

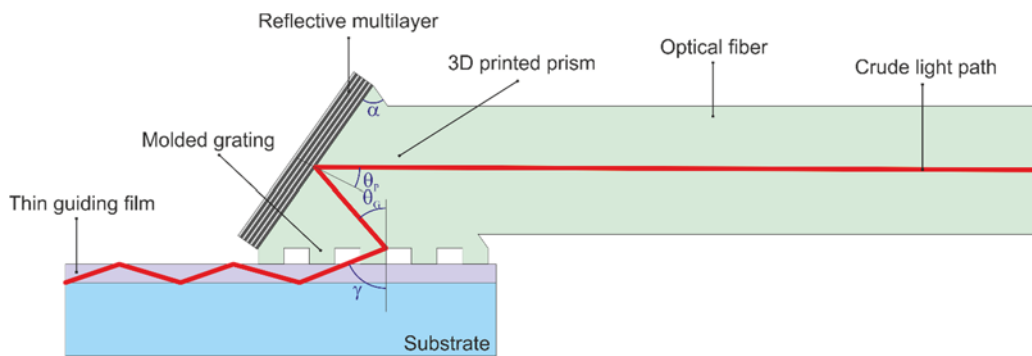


Figure 4.6: Design of a 3D printed coupler for fibre coupling from an optical fibre to a planar substrate through a thin waveguiding film. The optical fibre is placed parallel to the chip surface and is equipped with a microprism at the fibre end facet. For efficient redirection of light, the prism is covered with a reflective multilayer coating.

3D printed couplers as sketched in Figure 4.6 were investigated by numerical simulations only. These were carried out in order to obtain suitable design parameters for the implementation of the prism architecture, the multilayer grating and the attachment sites for the fibre. In Figure 4.7 an exemplary electromagnetic simulation of the coupling of light into a 3D printed couplers is shown. This simulation illustrates that the light coupling can efficiently occur with the current design. The simulation was carried out through Finite-Difference Time-Domain (FDTD) analysis.

The full electromagnetic analysis is required in the calculation because the sizes of the required structures are about the wavelength of incident light. Shown in the simulated image are the electric and magnetic fields relevant to the coupling architecture. Out-of-plane light propagating inside the incoming fibre is transferred into the underlying waveguiding layer where the propagating optical mode is excited. These simulations confirm matching analyses for mirror enhanced grating coupling structures as described in the previous subsection.

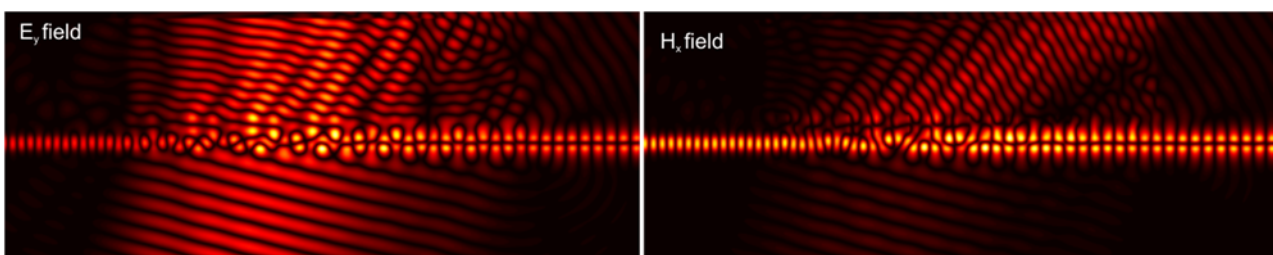


Figure 4.7: Electromagnetic simulation of the light coupling in 3D printed coupling devices.

Uncertainty estimation

For the experimentally realized devices, the statistical spread in performance was analysed by comparing several devices. For this purpose, identical couplers were fabricated on chip and each characterized in terms of insertion loss and coupling bandwidth, which are the key parameters for the use of the devices. The results are summarized in table 4.1:

Table 4.1 Statistical spread from comparison measurements of experimentally realised devices

	Insertion loss [dB]	Coupling bandwidth at 3dB [nm]
Mirror enhanced grating couplers	(-1.55 ± 0.4) dB	(28.34 ± 4.1) nm
Broadband 3D couplers	(-1.43 ± 0.6) dB	(128.5 ± 15.2) nm

4.4.4 Metrology in waveguide-based photonic devices

Key technical insight into the anisotropic properties of subwavelength metamaterials (SWG, i.e. periodic structures of alternating materials with a pitch much smaller than the wavelength of the propagating light, hence suppressing diffractive effects) has been gained, enabling to engineer the polarization-dependent properties of the SWG metamaterial by rotating the facets of its composing elements. The rotation angle of the segments with respect to the propagation direction was successfully demonstrated to critically affect TE modes while showing virtually no effects in TM modes. The capability of modifying the refractive effective index of TE modes maintaining the TM ones approximately constant, establishes a powerful tool to control the form birefringence of these type of meta-materials providing an easier fabrication since the duty cycle and the minimum feature size are fixed. This principle has been successfully applied to a MMI-based polarization splitter, a directional coupler polarization splitter and a polarization independent monomode waveguide.

Innovative silicon photonics devices have been developed, presenting compact footprint and enhanced performance through dispersion and anisotropy engineering provided by these structures. This approach enables to mitigate traditional drawbacks of this platform, such as its high birefringence, thermal dependence and sensitivity to fabrication errors. In particular, the following high-performance photonic devices for the SOI platform have been demonstrated:

- An integrated Fourier Transform microspectrometer for the near infrared with an experimentally demonstrated resolution down to 17 pm in a device of only 20 mm². The spectrometer comprises an array of 32 Mach–Zehnder interferometers implemented with microphotonic spirals with linearly increasing lengths up to 3 cm. Temperature drift mitigation techniques were applied in order to alleviate the stabilization constraints associated to the increased length, enabling a three-fold resolution increase compared to previous implementations based on microphotonic spirals. The device offers a remarkable potential for microsatellites, biological sensing or handheld spectroscopy.
- An integrated Fourier Transform microspectrometer adapted for the near infrared by reoptimizing SOI waveguide design. The spectrometer comprises a waveguide splitting tree feeding to an array of 42 Mach–Zehnder interferometers with linearly increasing optical path length differences. Two alternative implementations for power-splitting and optical delays have been demonstrated, adding to the versatility of the spectrometer for diverse applications in environmental sensing, breath analysis or stand-off detection for security. Resolutions under 3 nm and a free spectral range up to 57 nm were experimentally demonstrated.
- An ultra-broadband two-mode converter and de/multiplexer with insertion losses below 0.84 dB and crosstalk lower than -20.29 dB over an unprecedented bandwidth of 300 nm. The device is based on a sub-wavelength engineered multimode interference coupler, a 90° phase shifter and a symmetric Y-junction. Sub-wavelength grating waveguides enable dispersion engineering to further increase the bandwidth operation of conventional multimode interference coupler and, subsequently, of the mode de/multiplexer thereof. The overall footprint of the proposed device is only 36 μm x 3.7 μm. Furthermore, a novel broadband phase shifter, also based on SWG dispersion engineering was demonstrated.
- A broadband power splitter with -3 ± 0.5 dB polarization-independent transmission experimentally demonstrated in an unprecedented 390 nm bandwidth, even in the presence of waveguide width deviations as large as ± 25 nm. The device is based on modal engineering in slotted waveguides, with symmetric and adiabatic slot-to-strip transitions that prevent excitation of higher order slot modes. The proposed device simultaneously covers the O, E, S, C and L telecommunication bands, hence having the potential to become a key building block in numerous dual-polarization and broadband silicon photonics circuits

- A polarization splitter with an anisotropy-engineered MMI. The disparate effect of rotating the SWG structure on TE and TM modes enables to independently control the beat length of each polarization, hence reducing the length of the device without imposing any stringent fabrication requirement. The proposed polarization beam splitter presents an extinction ratio over 20 dB and insertion losses over 1.5 dB are achieved in a bandwidth of 116 nm for a device under 100 microns long.

Two new temperature-sensitive calibration and spectral retrieval methods have also been demonstrated for integrated Fourier transform microspectrometers, hence mitigating the stabilization requirements otherwise associated to resolution enhancements in this kind of devices. The first proposed algorithm is based on a temperature-sensitive calibration in which multiple calibration matrices are measured at different temperatures. For a correct selection of the calibration matrix, either a high precision measurement of the photonic chip temperature is performed, or the output interferogram of a reference input signal with a known spectrum is used. In the second proposed algorithm, phase errors in the calibration matrix are corrected by numerically shifting and aligning the MZIs transmittance functions. Indeterminations of the phase shift vector resulting from indistinguishable rising or descending flanks of the MZI transmittance function are solved by auxiliary interferogram measurements at two nearby temperatures.

This software athermalization was further complemented by two alternative hardware athermalization techniques for spatial heterodyne Fourier-transform (SHFT) microspectrometers have been performed. In the first technique, the SHFT interferometers are fully implemented with tilted subwavelength gratings, simultaneously providing polarization-independent behaviour and increased resilience to temperature changes. In the second technique, interferometers are implemented with conventional Si-wire waveguides, also including a SWG segment with perpendicular facets and a length compensation segment in one of the interferometer arm. Although this behaviour is polarization-dependent, a greater thermal effect mitigation is achieved for the selected polarization.

Furthermore, a novel spectral retrieval algorithm based on compressive sensing (CS) has been developed for SHFT devices. By advantageously applying the inherent incoherence between input and output basis of the FT scheme, sparse-spectrum signals can be retrieved in undersampling conditions (that is, with a reduced number of interferometers). This feature enables the reduction of device footprint and paves the way for spectral range expansion.

CSIC was the main developer of the described photonic devices and techniques, with support from JCM and WWU. In particular, WWU shared knowledge on efficient fibre-to-chip coupling. Efficient coupling leads to a higher power budget within the photonic chip, enabling a higher signal-to-noise ratio in the device characterization and a larger number of elements disposed in parallel in the MZI arrays. JCM provided access to JCMWave simulation software, which provides high-precision optical computation of complex waveguide structures. This is particularly useful when simulating non-conventional waveguide geometries, such as rotated SWG structures, which may not be accurately characterized by previously-available software.

4.4.5 Summary of key research outputs and conclusions

The project established metrology for optical printed circuit boards and contributed towards standardisation of key parameters, such as coupling loss, attenuation, crosstalk and BER, of short range interconnects. Novel fibre-to-chip couplers were developed to overcome existing barriers in conventional technologies. Moreover, the project studied a high-resolution Spatial-heterodyne Fourier Transform (SHFT) spectrometer, which most benefits from enhanced multi-fibre light coupling and metrology in integrated photonics.

A temperature chamber was set up to characterise the performance of the boards under different environmental conditions and BER measurements with accuracy levels of 0.001 were performed to investigate the thermal impact on data transmission. Observable changes were measured that correlated with the applied thermal load: increased thermal load to a section of waveguides showed a decrease in total attenuation and associated drop in the BER. The Encircled Flux measurements reveal a corresponding shift in the power distribution across the waveguides resulting in a compromising of the prescribed standardised EF limits. The research will have far reaching consequences for board designers, manufacturers and standardisation bodies.

For the high power characterisation at Watt level a set-up for the measurement of fibre connector transmission was built, and dependency of the connector performance on optical power investigated. It was observed that high quality connectors (AVIM, Mini-AVIM) kept their performance as specified at lower power when used at

Watt-level average power, but standard connectors (FC/APC) exhibited increased loss at powers over 300 mW. The target accuracy ($\pm 5\%$) was achieved for power levels exceeding 500 mW. A method for online core temperature measurement was successfully adapted for large mode area fibres and tested at over a hundred Watts in a thulium amplifier. A Good Practice Guide titled "Guidelines on measurement procedures for high power fibre optics" combines the results from all high power experiments.

Three different coupling architectures for injecting and extracting light from planar photonic chips were investigated: grating coupling structures for achieving high coupling efficiency with moderate coupling bandwidth, broadband coupling devices using adiabatic tapering for wide optical mode matching, as well as a combination of 3D architectures combining grating structures with 3D components. Simulations were performed to optimise the couplers. Coupling efficiency of up to 70 % with optical bandwidth of 30 nm was obtained for grating coupling devices and broadband transmission from visible to telecommunication wavelengths with minimum coupling loss of -1.4 dB was achieved for 3D adiabatic couplers.

For silicon photonics, several innovative devices with compact footprint and enhanced performance were developed using subwavelength metamaterials. The dispersion and anisotropy engineering provided by these structures enable to mitigate traditional drawbacks of this platform, such as high birefringence, thermal dependence and sensitivity to fabrication errors. In particular, an integrated Spatial-heterodyne Fourier Transform microspectrometer with a resolution down to 17 pm in a device of only 20 mm² was experimentally demonstrated, with a remarkable potential for microsatellites, biological sensing or handheld spectroscopy. New temperature-sensitive calibration and spectral retrieval methods were demonstrated for integrated Fourier transform microspectrometers, hence mitigating the stabilization requirements otherwise associated to resolution enhancements in this kind of devices. Other developed waveguide-based photonic devices include broadband mode multiplexers, power splitters and polarization splitters. Key technical insight into the anisotropic properties of sub-wavelength grating (SWG) structures was gained, enabling to engineer the polarization-dependent properties of the SWG metamaterial by rotating the facets of its composing elements. This principle was successfully applied to the polarization splitter based on multimode interference couplers, as well as to a directional coupler polarization splitter and a polarization independent monomode waveguide.

5 Impact

5.1 Dissemination

The project results were disseminated widely to the stakeholder community via publications conferences conferences, training events, workshop and project website.

The project partners have generated 11 open-access peer-reviewed papers, 4 published proceedings and, more than 50 conference presentation (talks and posters).

The project partners had about 20 different training events for project partners and for wider audience.

In spring 2018, a two-day workshop was held to disseminate the project's results to all the interested industrial and academic parties as a special session at SPIE Photonics West Conference: The PhotIND topics were divided under two sessions; Session 6: "Applications and Metrology" and Session 8: "Special Session: PHOTIND EMPIR European Project". The number of attendees was 50–60.

The PhotInd website (<http://www.photind.eu/>) was launched at the beginning of the project. At the end of the project time, the website had received more than 14 000 visits.

A Good Practice Guide titled "Guidelines on measurement procedures for high power fibre optics application and calibration of non-conventional sensors" was developed by the project and is available for download on the project website.

5.2 Impact on industrial and other user communities

The manufacturers of advanced optical fibres will benefit from the project through the availability of novel tools for high-level characterisation of dimensional and optical properties. The development of techniques for online monitoring and control of the fabrication process will have a significant impact on the fibre industry, which would improve the quality of the production, increase the yield of the processes and reduce costs. The online fibre characterisation device development within the project is an interesting tool for the fibre drawing quality control. A fibre manufacturing producer has presented interest on the method.

Characterizing the wavelength-dependent phase delay induced by optical fibre (both single or multimode) in broad spectral range using SEA TADPOLE interferometer allows to measure dispersion and spatial distribution of different modes of ca 1 m long fibres. In case the implementation is successful, the technique is of great scientific and practical interest for speciality fibre characterization.

The development of new calibration techniques for the latest generation fibre optics will benefit industrial applications in the field of sensors. High-resolution spatial measurements of distance and attenuation scale calibrations would improve the accuracy of sensors.

The developed EAF measuring instrument is planned to be for sale by one of the project partners. This will allow industry to better characterise output properties of different fibres.

New measurement method for cladding light content has already been implemented, allowing identification of pedestal light content in more complex fibres. Test are being made to use the method for industrial product characterization.

Numerical methods for simulating measurement setups for dimensional characterisation of optical fibres have proven high efficiency and accuracy in the project. Interfaces to these methods will be implemented in the commercial software package JCMSuite.

Finite-element based numerical methods for simulating fibre chip coupling are found to perform very well for problems with large computational domains. The problem to optimize the device is a high-dimensional optimization problem. Methods to solve the optimization problem efficiently have been tested. These will be part of the commercial software package JCMSuite.

Numerical methods for accurately computing overlap integrals of diverse finite-element simulation results representing optical modes in optical fibres have been shown high efficiency. An interface to compute the integrals directly from the FEM solution without prior export to a regular mesh to be implemented in the commercial solver JCMSuite and to be transferred to the user community of this tool.

The innovative silicon photonic devices developed within the project (namely the SHFT microspectrometer and the auxiliary devices as polarization controllers and mode multiplexers) offer a remarkable opportunity for technological transfer. This is showcased by the recent creation of the spin-off company Alcyon Photonics,

which is already licensing two of the national patent applications ("Integrated mode converter and multiplexer" and "Integrated polarization beam splitter") created within this project, and is in the process of licensing the third one ("Waveguide, fabrication method thereof and polarization beamsplitter using said waveguide"). All patents will be extended to international PCT applications within 12 months of their submission dates.

CSIC submitted two national patent applications regarding distributed fibre sensing: "System and method of distributed scattering profile characterisation of an optical fibre" and "System and method of distributed characterisation of refractive index variations of an optical fibre". Both patents submission are under examination and have been extended internationally through PCT applications. Both patents will be licensed to co-applicant FOCUS (Fiber Optics Consulting Services and Technologies S.L.) a spin-off company, which incorporates in their products our earlier OTDR developments and has already declared their interest on both patented technologies to enhance the performance of their optical reflectometry equipment. FOCUS will exploit the results by integrating the technologies proposed in the patents into their two commercial products, hence improving their sensitivity and resolution: FINDAS (distributed acoustic sensor) and FINEST (distributed temperature and strain sensor).

The consortium collaborated closely with companies interested in the results of the project. Several companies were in the project stakeholder committee and ten participated in the stakeholders meetings. Also the co-operation with the European Photonics Industry Consortium (EPIC) and European Optical Society Biennial Meeting (EOSAM) guarantees effective dissemination.

At the end of the project, a formal questionnaire was distributed to the industrial partners and the collaborators to determine the uptake of the project outcomes by the photonic industry. The most useful project outcomes for the stakeholders were: "Measurement techniques for characterisation of advanced optical fibres and photonic components", also "Artefacts for the calibration of high resolution optical reflectometers (OTDR and OLCR)" were rated positive. A report on the uptake of project outcomes by the photonics industry, along with recommendations on how to increase the uptake was written containing results from the questionnaire and an exploitation plan for the key outputs.

5.3 Impact on the metrology and scientific communities

A better understanding of the optical properties of advanced optical fibres will benefit the fibre optic community. Especially, new techniques for AEF and OTDR high resolution measurements requires a deep analysis of optics, optical detection and image processing; the outcomes of which will be beneficial for the scientific communities. Results from intercomparisons of OTDR measurements and comparisons between modal distribution simulations and measurements will be shared with the metrological community.

In particular, the advances in fibre-to-chip light coupling and photonic metrology provided by this project will be used in many areas of integrated photonic circuits. By simplifying light coupling and providing a better waveguide characterisation, scientific communities will be able to focus their effort on the actual chip functionalities, increasing research efficiency and impact.

Terahertz communications is now at the research stage, focusing significant attention from the scientific community. Given its novelty, metrological communities still need to develop appropriate characterisation systems and standards. The results of the project will therefore greatly benefit all the aforementioned parties.

The developed methods to establish traceability will be a key part in the development of new photonics measurement techniques.

~~An absolute cryogenic electric substitution standard radiometer as a new primary standard for calibration of fiber-optics power meters with lower uncertainty was implemented at GMI.~~

The following new calibration services were established as a result of the project:

- Simultaneous resolution and temperature calibration of distributed fibre sensors; available at CSIC commercial calibration services.
- Fibre Bragg grating interrogator calibration based on a tuneable simulated Bragg grating, available at CSIC commercial calibration services.
- Fibre Bragg grating interrogator calibration based on calibrated absorption gas cells; available at CSIC commercial calibration services.
- Traceable Encircled Angular Flux calibrations in multimode optical fibre systems. METAS will provide calibration services based on this new development.
- Artefact for the calibration of the distance scale of OLCR. METAS will provide calibration services using these artefacts and disseminate them to interested calibration laboratories.

- Artefact for the calibration of the distance scale of high-resolution OTDR. METAS will provide calibration services using these artefacts and disseminate them to interested calibration laboratories.
- Artefact for the calibration of the attenuation scale of multimode OTDR. METAS will provide calibration services using these artefacts and disseminate them to interested calibration laboratories.
- Low uncertainty calibration of fibre optics power meters on absolute cryogenic standard radiometer. CMI provides calibration services.

5.4 Impact on relevant standards

This project has had an impact on the work of IEC standardisation groups together with metrology committees of CCPR and EURAMET TC-PR. Project partners have taken part in at least 16 different technical committee meetings. Project partners have provided advice for the updating of existing standards and contribute to new standards related to the calibration of fibre optics measuring instruments (IEC TC86, WG4) and to the functional performance of short range interconnects (IEC TC86/TC91, JWG9).

The project partners provided advice for the improvement of calibration techniques to CCPR task groups on fibre optics (TG6) and on OTDR length calibration (TG9).

The performance of EAF measurements were validated by an inter-comparison, which showed excellent results. Arden and METAS wrote a report including an uncertainty estimation on the system for traceable EAF measurement. Discussions have been carried out with the technical committee IEC/TC86/SC86B/WG4, which is in charge of developing the relevant standards for EAF measurements and need to be further pursued. Jointly with the Swiss IEC TC86 committee (TK86) METAS will disseminate the results of our activities on EAF measurements within the IEC TC86/SC86B/WG4 in the form of a report or of a presentation, after the end of the project. Arden will send the report and uncertainty budget to the coordinator for submission to EURAMET. For more information see Deliverable Report D6, Task 3.1

As the technology rapidly develops, there is a corresponding need to provide characterisation of the optical printed circuit boards for the key operational parameters such as attenuation, isolation (crosstalk) and bit error ratio (BER) as well as a need to provide standardisation through dissemination to the international standards bodies. This work informs the standards development within the International Electrotechnical Commission (IEC), principally through the work of the IEC technical committee 86, improving the standardisation of key measurements as well as making use of recently the proposed adoption of a reliable measurement definition system for optical interconnect (62496-2:2017 (E) - Optical circuit boards - Basic test and measurement procedures - Part 2: General guidance for definition of measurement conditions for optical characteristics of optical circuit boards. The work will be presented to the relevant national committees GEL/86/2 and 3, that feed into the international IEC JWG9 Optical functionality for electronic assemblies) under TC86. This research has far reaching consequences for electro-optical printed circuit board designers, manufacturers and standards bodies. The unavoidable increase in board complexity and hybridization, in the drive to accommodate higher and higher data rates, will need to take into account these performance and functional limitations imposed by the application of thermal loading.

5.5 Longer-term economic, social and environmental impacts

The worldwide photonics market was 447 billion Euro in 2015 and it is expected to grow to 615 billion Euro in 2020. A global market share of 15.5 % makes Europe the world's second-biggest supplier of photonics, after China. European Photonics Production has increased by over 62 % over the last 10 years, which is much stronger growth than industrial production in Europe in general. Similar to electronics, photonics products are used products in a wide range of sectors of which production technology, optical measurements & image processing and optical communication & information technology are the most important ones.

The development of the optical fibre characterisation techniques, efficient photonic interconnects and metrology instruments in this project will undoubtedly benefit this ever-growing industry, strengthening European competitiveness and increasing its total turnover.

Reliable high power characterisation of fibre components will enable more reliable laser-based production methods. This will lead to reduced costs and thus make precision-engineered items available to a wider audience. Examples include miniaturised medical devices, components in automobile construction and functionalisation of surfaces.

The advances in optical fibres and their manufacture as well as better characterisation of transmission links will improve the whole communication infrastructure, which will have a positive effect on the economy and European citizens, for example via Fibre-To-The-Home.

Optical communication infrastructure is the most environmentally friendly method for data transfer. Replacing metal wire based local connections with optical connections (Fibre-To-The-Home) will reduce energy consumption while increasing bandwidths. Furthermore, data interconnects in super-computers require colossal amounts of energy that limit their operation and significantly impact the environment. By providing efficient and low-power all-optical interconnects, this hazard would be greatly reduced.

6 List of publications

1. V. Velasco, J. Galindo-Santos, P. Cheben, M. L. Calvo, J. Schmid, A. Delage, D.-X. Xu, S. Janz, P. Corredera, "Temperature drift compensation in Fourier-transform integrated micro-spectrometers", *Optica pura y aplicada* **48**, 283–289 (2015), doi: <http://dx.doi.org/10.7149/OPA.48.4.283>
2. M. Nedeljković, A. V. Velasco, A. Khokhar, A. Delage, P. Cheben, and G. Mashanovich, "Mid-Infrared Silicon-on-Insulator Fourier-Transform Spectrometer Chip", *IEEE Photonics Technology Letters* **28**, 528–531, doi: <https://doi.org/10.1109/LPT.2015.2496729>
3. I. Fatadin, "Estimation of BER from Error Vector Magnitude for Optical Coherent Systems", *Photonics* **3**, 21 (2016). doi: <https://10.3390/photonics3020021>
4. D. González-Andrade; J. G. Wangüemert-Pérez; A. V. Velasco; A. Ortega-Moñux; A. Herero-Bermello; I. Molina-Fernández; R. Halier; P. Cheben, "Ultra-broadband mode converter and multiplexer based on sub-wavelength structures", *IEEE Photonics Journal* **10**, (2018). doi: <http://dx.doi.org/10.1109/JPHOT.2018.2819364> .
5. A. Herrero-Bermello, A. V. Velasco, H. Podmore, P. Cheben, J. H. Schmid, S. Janz, M. L. Calvo, D.X. Xu, and P. Corredera, "Temperature dependence mitigation in stationary Fourier-transform on-chip spectrometers", *Optics Letters* **42**, 2239–2242, (2017). <https://doi.org/10.1364/OL.42.002239>
6. H. Podmore, A. Scott, P. Cheben, A.V. Velasco, J. H. Schmid, M. Vachon, and R. Lee, "Demonstration of a compressive-sensing Fourier-transform on-chip spectrometer", *Optics Letters* **42**, 1440–1443 (2017), <https://doi.org/10.1364/OL.42.001440>
7. José Luis de Miguel, Juan Galindo-Santos, Concepción Pulido de Torres, Pedro Salgado, Pedro Corredera y Aitor V. Velasco, Experimental, "Demonstration of Low-Uncertainty Calibration Methods for Bragg Grating Interrogators", *Sensors* **18**, 1895 (2018), <https://doi.org/10.3390/s18061895>
8. Franz Beier, Marco Plötner, Bettina Sattler, Fabian Stutzki, Till Walbaum, Andreas Liem, Nicoletta Haarlammert, Thomas Schreiber, Ramona Eberhardt, and Andreas Tünnermann, "Measuring thermal load in fiber amplifiers in the presence of transversal mode instabilities," *Optics Letters* **42**, 4311–4314 (2017), doi: <https://doi.org/10.1364/OL.42.004311>
9. Irshaad Fatadin, "Calibration of Estimated BER from Error Vector Magnitude with Carrier Phase Recovery", *Recent Adv. Photonics Opt* **1**, 1–6 (2017), <http://scholarlypages.org/Articles/photonics-and-optics/rapo-1-001.pdf>
10. Muluneh G. Abebe, Aimi Abass, Guillaume Gomard, Lin Zschiedrich, Uli Lemmer, Bryce S. Richards, Carsten Rockstuhl, Ulrich W. Paetzold, "Rigorous wave-optical treatment of photon recycling in thermodynamics of photovoltaics: Perovskite thin-film solar cells", *Phys. Rev. B* **98**, 075141 (2018), doi: <http://dx.doi.org/10.1103/PhysRevB.98.075141>
11. José Manuel Luque-González, Alaine Herrero-Bermello, Alejandro Ortega-Moñux, Íñigo Molina-Fernández, Aitor V. Velasco, Pavel Cheben, Jens H. Schmid, Shurui Wang, Robert Halir, "Tilted subwavelength gratings: controlling anisotropy in metamaterial nanophotonic waveguides" *Optics Letters* (approved, waiting publication)
12. M. Hammerschmidt, et al., Quantifying parameter uncertainties in optical scatterometry using Bayesian inversion, *Proc. SPIE* **10330**, 1033004 (2017); doi: <https://doi.org/10.1117/12.2270596>
13. N. Castagna, J. Morel, L. Testa, S. Burger, "Modelling of standard and specialty fibre-based systems using finite element methods", *Proc. SPIE* **10683**, 1068336 (2018), doi: <https://doi.org/10.1117/12.2307372>.
14. N. Castagna, J. Morel, E. Robinson, H. Yang, "Traceable instruments for Encircled Angular Flux measurements", *Proc. SPIE* **10683**, 106831B (2018), doi: <https://doi.org/10.1117/12.2306430>.
15. M. Shpak, S. Burger, V. Byman, K. Saastamoinen, M. Haapalainen, A. Lassila, "Online measurement of optical fibre geometry during manufacturing," *Proc. SPIE* **10683**, 1068318 (2018), doi: <https://10.1117/12.2314762>
16. T. Walbaum, A Liem, T. Schreiber, R. Eberhardt, A Tünnermann, "Measurement and removal of cladding light in high power fiber systems", *Proc. SPIE* **10513**, 1051330 (2018), doi: <https://doi.org/10.1117/12.2288266>

17. J.Galindo, Metrología óptica de frecuencias. Síntesis, análisis y aplicación de referencias ópticas, PhD, doi: https://repositorio.uam.es/bitstream/handle/10486/682698/galindo_santos_juan_francisco.pdf

7 Website address and contact details

Website address: <https://www.photind.eu/>

Information on the project (project description, events, publications, newsletters, reports, etc.) for partners and stakeholders



Contact details

For further information on

- dimensional and optical characterisation of advanced optical fibres, contact Maksim Shpak, VTT, maksim.shpak@vtt.fi
- metrology in waveguide-based photonic devices, contact Aitor Villafranca, CSIC, a.villafranca@csic.es
- distributed and quasi-distributed fibre sensors, contact Pedro Corredera, CSIC, p.corredera@csic.es
- absolute primary standard radiometer for optical fibre power measurement, contact Marek Šmíd, CMI msmid@cmi.cz
- metrology for high power fibre optics, contact Till Walbaum, FhG, Till.Walbaum@iof.fraunhofer.de
- fibre to chip couplers, contact Wolfgang Pernice, WWU, wolfram.pernice@uni-muenster.de.
- optical waveguides under different environmental conditions, contact Robert ferguson, NPL, Robert.ferguson@npl.co.uk
- characterisation of THz transmission links, contact, Mira Naftaly, NPL, mira.naftaly@npl.co.uk
- traceable system for Encircled Angular Flux measurements, contact Edward Robinson, Arden, ed.robinson@ardenphotonics.com
- traceable calibration of OTDRs, contact Jacques Morel, METAS, Jacques.morel@metas.ch